J. Earth Syst. Sci. (2022)131 211
https://doi.org/10.1007/s12040-022-01951-9

Simulated dynamics and thermodynamics processes leading to the rapid intensification of rare tropical cyclones over the North Indian Oceans

Arpita Munsi[1,2], Amit Kesarkar[1,*], Jyoti Bhate[1], Kasturi Singh[1], Abhishek Panchal[1], Govindan Kutty[2] and Ramkumar Giri[3]

[1]*National Atmospheric Research Laboratory, Department of Space, Govt. of India, Gadanki, Chittoor District, Andhra Pradesh 517 112, India.*
[2]*Indian Institute of Space Technology, Valaimala, Thiruvananthapuram, Kerala 695 547, India.*
[3]*India Meteorological Department, Mausam Bhavan, Lodhi Road, New Delhi, India.*
**Corresponding author. e-mail: amit@narl.gov.in amit.kesarkar@gmail.com*

MS received 28 December 2021; revised 21 March 2022; accepted 24 April 2022

The life cycle dynamics and intensification processes of three long-duration tropical cyclones (TCs), viz., Fani (2019), Luban (2018), and Ockhi (2017) formed over the North Indian Ocean (NIO) have been investigated by developing a high-resolution (6 km × 6 km) mesoscale analysis using WRF and En3D-VAR data assimilation system. The release of CAPE in nearly saturated middle-level relative humidity caused intense diabatic heating, leading to an increase in low-level convergence triggering rapid intensification (RI). The strengthening of the relative vorticity tendency terms was due to vertical stretching (TC Fani) and middle tropospheric advection (TCs Luban and Ockhi). The increase or decrease in upper-tropospheric divergence led to RI through two different mechanisms. The increase in upper divergence strengthens the vortical convection (in TC Luban and Fani) by enhancing the moisture and heat transport, whereas its decrease caused a reduction in the upper-level ventilation flow at 200 hPa followed by moisture accumulation, enhanced diabatic heating, and strengthened the warm core (TC Ockhi). The RI caused the vortex of three cyclones to extend up to the upper troposphere. The well organised wind during RI led the unorganised, weak, discontinuous vertical vortex columns to become organised with intense vertical velocity throughout the column. Spatial distributions of Okubo–Wiess (OW) parameter showed TC core dominated by vorticity than strain, since deep depression (DD) stages.

Keywords. Mesoscale modelling; tropical cyclone; rapid intensification; vortical advection; vortex stretching; asymmetrisation; axisymmetrisation.

1. Introduction

Tropical cyclones (TCs) are one of the most threatening weather-related hazards on Earth that causes loss of lives and property. They are associated with very intense rotating wind and precipitation. Due to advancements in numerical weather prediction models and satellite observations, the accuracy of a TC's forecast, especially the skill of TC track forecast, has increased reasonably. However, improvement in forecasting

Published online: 28 September 2022

skills for TC intensity still remains challenging (Wang and Chan 2002; DeMaria *et al.* 2014). The operational intensity forecast error for the intense TCs (wind speed >48 knots) is considerably large over the NIO region (Nadimpalli *et al.* 2021). To improve the forecasting skill of TC intensity, understanding the dynamics of TC intensification is essential. Formation of TC concomitant with the kinetic and thermodynamic physical process occurs on a convective to synoptic scale. Therefore, the development of understanding the contributions of the multiscale processes causing cyclogenesis and rapid intensification is essential. The in-up-out circulation in a convective region is associated with low to mid-level convergence and upper-level divergence (Tory and Frank 2010). The low-level convergence ensures the continuous supply of water vapour, mass, and momentum to maintain the cumulus convection, and thus it acts as a pump primer ingredient (Gray 1975). The large magnitude of low-level relative vorticity is one of the prime requirements for TC genesis (Gray 1968). Hendricks *et al.* (2004) and Montgomery *et al.* (2006) have proposed vortical hot tower (VHT) as a route to cyclogenesis. Rajasree *et al.* (2016a, b) have also studied the role of VHT in cyclogenesis and concluded that the aggregation of vorticity and moisture in terms of VHT plays a vital role in cyclogenesis in North Indian Oceans (NIO). Dunkerton *et al.* (2009) have proposed a turbulence cascading mechanism which gives rise to a large disturbance like TC. This mechanism is popularly known as a marsupial paradigm. The hypothesis of the paradigm indicates that the genesis of TCs occurs from the atmospheric waves where quasi-Lagrangian cyclonic circulation (QLCC) protects the incipient disturbance from the dissipative forces present in the environment. The marsupial paradigm explains the formation of warm core and thus the TC.

The concept of QLCC is similar to the concept of the cat's eye in fluid dynamics. These circulations allow mass/energy to enter inside the system and not escape in the horizontal direction. Therefore, it aggregates mass/energy within the circulation. In TCs, the moisture and vorticity from meso-α scale aggregated inside quasi-Lagrangian cyclonic circulation. The aggregation of vorticity inside the QLCC causes the development of VHT (Hendricks *et al.* 2004; Montgomery *et al.* 2006) or cumulus congestus clouds (Wang 2012, 2014). Dunkerton *et al.* (2009) have also indicated that the latent heat released during condensation inside the cloud (meso-γ scale energy) contributes to the warm core formation that causes intensification of the system. This intensification leads to the formation of large-scale disturbances like TC. Rajasree *et al.* (2016a, b, 2021) have studied the marsupial paradigm's applicability over NIO and indicated that the low-pressure system generated from disturbances embedded in the atmospheric waves over the equatorial Indian Ocean (IO) develops as a TC.

The intensity of TC is governed by many complex physical mechanisms of the ocean, atmosphere, and their interactions. The TC intensity and structure changes are associated with complex boundary layer (BL) forces of different scales (Wang and Wu 2004). The interactions among spiral bands, eyewall process, dynamics of vortex Rossby waves, embedded mesoscale vortices moderate the internal dynamics during TC life cycles. The eyewall usually contracts during TC intensification (Willoughby *et al.* 1982). The axisymmetric disturbances of a vortex involve outward propagating Rossby-wave vortex where restoring force comes from the radial gradient of storm vorticity (Montgomery and Kallenbach 1997). The environmental control on TC includes environmental flow, vertical shear of horizontal wind, beta effect, interaction with other TC, and upper-tropospheric trough. Strong environmental flow relative to TC motion contradicts TC intensification (Merrill 1988).

On the other hand, small asymmetry in the lower level helps the TC intensify through the symmetric distribution of low-level moisture convergence and surface fluxes (Peng *et al.* 1999). When the eddy momentum flux convergence is >10 ms^{-1} day^{-1} (calculated over the region of 300–600 km radius), it is attributed as an upper-level air trough interaction that weakens a TC (Hanley *et al.* 2001). Persing *et al.* (2013) have studied the role of intensification process in asymmetric and axisymmetric dynamics in TC's evolution. Their study indicated that the study of asymmetric–axisymmetric dynamics at the maximum intensification (MI) stage is vital. Here, the maximum intensification stage is specified as the duration when the TCs attained their maximum sustained surface wind speed. Smith and Montgomery (2015) reviewed the paradigm of TC intensification to explore the relationship between the radius of maximum tangential wind and intensification. Their study challenged the convective ring model based on the axisymmetric framework. They argued that the representing

intensity of TC in terms of maximum wind radius has limitations as it is not materially conserved quantity and not fundamental to the spin-up process. Nevertheless, the physical mechanism involved in the TC intensification process needs a better theoretical understanding and requires more investigation.

The dynamical process which leads the TC to rapid intensification (RI) still remains ambiguous. Previous studies identified the favourable conditions for RI as anomalously warm SST, weak vertical shear of horizontal wind, high lower tropospheric relative humidity, and weak forcing from the upper-level trough. Kieu and Zhang (2009) showed that the rate of rotational flows in the TC inner-core increases exponentially. Kaplan *et al.* (2010) analysed that vertical wind shear and upper-level divergence have the relatively highest weights in predicting the RI of TCs over the Atlantic basin. Zhang and Chen (2012) hypothesised that the divergent outflow at the upper level favours warm-core generation by protecting it from the environmental flow ventilation. Miyamoto and Nolan (2018) analysed that the indicative characteristics of onset of RI are the decrease of radius of maximum tangential wind, i.e., increase in Rossby number, symmetrisation of flow structure, reduction in vortex tilt, and approach of the radius of maximum convergence to the radius of maximum wind. Chen *et al.* (2019) studied that reduction of above BL ventilation helps in accumulating the energy within the inner core, leading to RI.

Most of the previous research articles have studied the dynamical and thermodynamical effect on TC intensification and have analysed the TCs formed over the Atlantic and North Pacific oceans. The NIO basin, bounded by the continents, differs from the other TC basins owing to its shallow depth and the low flat coastal terrain that produce much larger devastation (Singh *et al.* 2019). In addition, the NIO basin is a comparatively smaller ocean basin, and consequently, the lifespan of the systems formed over it is relatively less than the hurricanes and TCs formed over other world ocean basins. However, in a relatively short span of life period, the NIO TCs frequently encounter RI. A limited number of studies (Kotal and Bhowmik 2013; Bhalachandran *et al.* 2019; Singh *et al.* 2020; Routray *et al.* 2020; Singh *et al.* 2021) have analysed the TC evolution from the aspect of dynamical and thermodynamical behaviour over NIO. Kotal and Bhowmik (2013) showed that TC atmospheric environment plays a vital role in the TC intensification process. Routray *et al.* (2020) analysed the pre- and post-genesis characteristics of TC Fani and studied the dynamic and thermodynamic features at the different stages of the TC. Prediction of TC Fani genesis near the equator in 48 hrs advance and RI were examined by Singh *et al.* (2020). They also showed that RI was mostly controlled by warm SST and 'anomalous warm core eddies'. In the past few years, NIO has experienced more rapidly intensified TCs due to rapidly warmed NIO associated with the warming climate (Singh and Roxy 2022). Indian coastal states are densely populated and are in low socio-economic conditions. The increasing number of rapidly intensified cyclones caused heavy loss of lives and infrastructure in recent years. Further rise in the frequency of RI TCs over NIO in the changing climate scenario may cause a further rise in the death toll and destruction. To reduce the loss caused by these systems, accurate prediction of intensity at every phase of TC life is inevitable.

Therefore, the present work analyses the dynamical and thermodynamical behaviour of TC intensification, particularly RI of three TCs cases, viz., Fani (2019), Luban (2018), and Ockhi (2017) formed over NIO. The system Fani formed near the equator (2.7°N) region of Bay of Bengal (BoB), which is rare in any ocean basin and is the most intense pre-monsoonal RI TC crossing Odisha coast with a maximum sustained wind speed of $\sim$116 knots. The Morphed Integrated Microwave Imagery (MIMIC) TC report indicated that Fani went through an eyewall replacement cycle when it approached the Odisha coast. The TC Luban was the case where it was expected that the system would weaken under unfavourable atmospheric conditions during genesis. However, the system underwent RI from 9 to 10 October 2018. Finally, TC Ockhi was a rare case with RI in the genesis stage. Within six hours, it intensified from deep depression into a cyclonic storm over Comorin sea (oceanic region south of Kerala and Tamil Nadu and west of Sri Lanka). The primary objective of this manuscript is to bring attention to the vastly different environments and internal dynamics experienced by rapidly intensifying TCs over the NIO basin within a relatively short period by using Weather Research and Forecasting (WRF) model simulated high-resolution mesoscale analysis. The used data and methodology are described in section 2. The results are discussed in section 3, and in section 4, we concluded our study.

2. Mesoscale modelling and experimental details

We have used the high-resolution (6 km × 6 km) mesoscale analysis developed using the dynamical downscaling technique. The mesoscale model WRF and hybrid ensemble-3DVar (En3DVAR) data assimilation techniques have been used to carry out the study. WRF model and WRFDA modelling system have been obtained from NCAR (available at https://www.mmm.ucar.edu/weather-research-and-forecasting-model). The model configuration used in the present study are the Unified NAOH land Surface Model, Rapid Radiative Transfer Model (RRTM) for longwave radiation scheme, Dudhia scheme for shortwave radiation scheme, Thompson scheme for microphysics parameterisation, Turbulence Kinetic Energy (MYJ TKE) scheme for the planetary boundary layer, Kain–Frisch scheme for cumulus physics. For assimilation, the prepbufr dataset containing surface and upper air observation has been obtained from NCAR's Research Data Archive (RDA; https://rda.ucar.edu/). In addition, OSCAT-2 (Ocean Scatterometer-2) scatterometer wind data (Scatsat-1 obtained from https://www.mosdac.gov.in and ASCAT (Advanced Scatterometer) obtained from https://rda.ucar.edu/), radiometer (Windsat obtained from www.rmss.com) wind data, and the GDAS (Global Data Assimilation System) radiance data (https://rda.ucar.edu/) have been assimilated to obtain the improved analysis. The model has been initialised with Global Forecast System (GFS) model analysis available from National Centre for Environmental Prediction (NCEP) at 0.5°×0.5° horizontal resolution (https://www.ncei.noaa.gov/data/global-forecast-system/access/historical/analysis). The background error (BE) statistics for data assimilation were created using the National Meteorological Centre method (Barker *et al.* 2004). The model integration was done for 12 hrs. *In-situ,* radiance and scatterometer data (details shown in table 1) were assimilated in cyclic mode at every 6 hrs at synoptic times, i.e., 00, 06, 12, and 18 UTC. The assimilation window was ±3 hrs from the initial conditions. The mesoscale reanalysis was prepared in warm start mode. The mesoscale reanalysis starts from the depression stage to the dissipation stage of the cyclone.

The details of the track, intensity, and rainfall validation have been presented in our companion paper (Munsi *et al.* 2021) and found that developed mesoscale analysis successfully simulates TCs' life cycle, including position, intensity, and rainfall. The root mean square error (RMSE) of observation-background (O-B) and observation-analysis (O-A) are plotted in figure 1. Here the background means the initial conditions before the assimilation. The RMSE in the O-A is less than the same in O-B for all the three TCs, as observed in figure 1. Similar results were found in our earlier study Bhate *et al.* (2021). The validation of winds and structure has also been discussed in the companion paper (Munsi *et al.* 2021). The simulation of this paper also indicates that the structures of the TCs are well simulated in the mesoscale analysis. Apart from the parameters such as convective available potential energy (CAPE), vertical velocity, and relative humidity, the following parameters calculated from the mesoscale analysis have been used to understand the dynamics and thermodynamics associated with the TCs evolution.

- The TC's spin-up is defined as the azimuthally averaged maximum wind over the cyclonic circulation region (Sanger *et al.* 2014). The spin-up has been calculated at the height of 850 hPa. At every 6 hourly intervals from the genesis time, the maximum wind at increasing radii from the TC centre is considered. We have calculated the maximum wind at each radius up to 540 km with an interval of 36 km from the centre of TC, and then it is averaged over all radii. This quantity is defined as the spin-up of the TC.
- Relative vorticity is generated due to the horizontal wind gradient. Positive relative vorticity and convection lead to divergence at the upper troposphere during the lifecycle of the TC. Relative vorticity: $\zeta = (\frac{\partial v}{\partial x} - \frac{\partial u}{\partial y})$, where u and v are the zonal and meridional wind components, respectively.
- The equation for the vorticity balance for the compressible flow can be derived from the compressible momentum equation written below.

$$\frac{D\mathbf{V}}{Dt} = -2\boldsymbol{\Omega} \times \mathbf{V} - \frac{\nabla P}{\rho} + \nabla \boldsymbol{\Phi} + \mathbf{F}, \qquad (1)$$

where $\boldsymbol{\Phi}$ is the gravitational potential, $\mathbf{F}$ is the sum of frictional and turbulence forces per unit mass. The $\frac{D\mathbf{V}}{Dt} = \frac{\partial \mathbf{V}}{\partial t} + (\mathbf{V} \cdot \nabla)\mathbf{V} = \frac{\partial \mathbf{V}}{\partial t} + \frac{1}{2}\nabla(\mathbf{V} \cdot \mathbf{V}) - \mathbf{V} \times (\nabla \times \mathbf{V})$ represents the total derivative of the velocity for compressible flow (using identity

Table 1. *The data assimilated for generating mesoscale analysis.*

Data	Sensors
Global Data Assimilation System (GDAS) dataset	• Infrared Atmospheric Sounding Interferometer • Advanced Microwave Sounding Unit-B • Advanced Tech Microwave Sounder • Global Positioning System (GPS) radio acclusion • Microwave Humidity Sounder, Atmospheric Infrared Sounder • The surface level and upper level observations in prepBUFR format
Scatterometer/Radiometer winds observation	• OSCAT-2 • ASCAT • Windsat

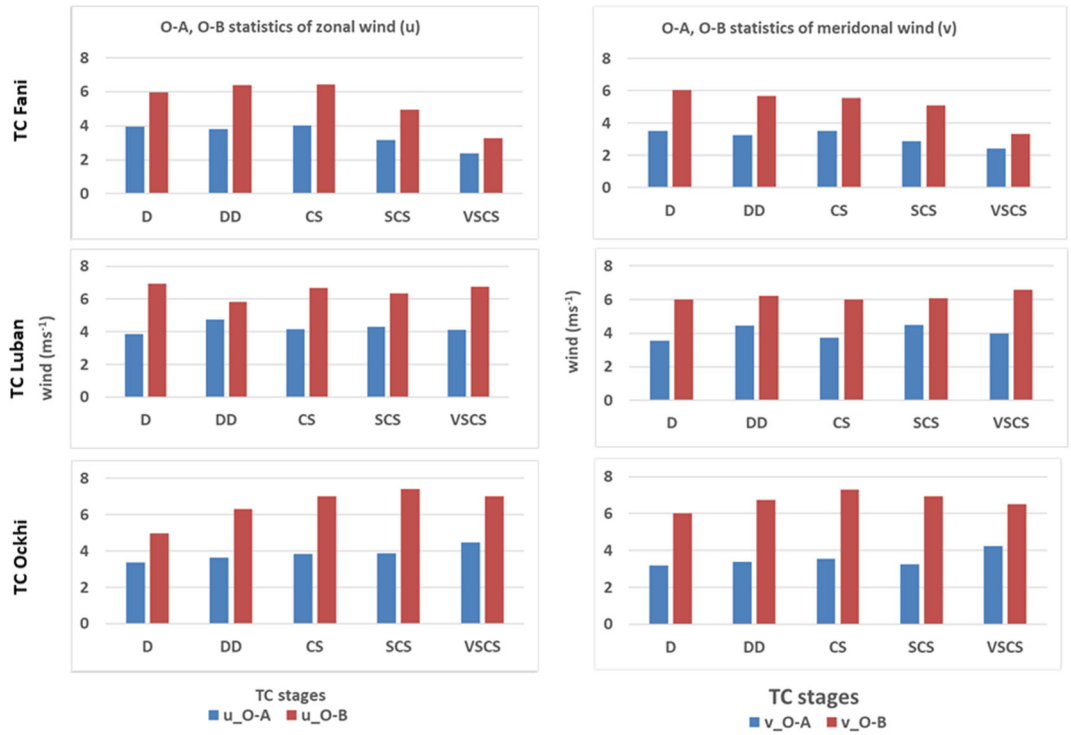

Figure 1. O-A and O-B statistics of zonal wind (u; first column) and meridional wind (v; second column) of TC Fani (first row), Luban (second row), and Ockhi (third row) at the different stages of TCs.

$\frac{1}{2}\nabla(A\cdot B)=(A\cdot\nabla)B+A\times(\nabla\times B)$). The vorticity balance equation can be derived by operating curl on both sides of equation (1) and substituting ($\zeta=\nabla\times\mathbf{V}$). The left-hand side of equation (1) can be simplified to obtain the following form.

$$\nabla\times\frac{D\mathbf{V}}{Dt}=\nabla\times\frac{\partial\mathbf{V}}{\partial t}+\nabla\times\left\{\frac{1}{2}\nabla(\mathbf{V}\cdot\mathbf{V})-\mathbf{V}\times\zeta\right\}$$
$$=\frac{\partial\zeta}{\partial t}+(\nabla\cdot\zeta)\mathbf{V}-(\nabla\cdot\mathbf{V})\zeta,$$

where $\nabla\times\frac{1}{2}\nabla(\mathbf{V}\cdot\mathbf{V})=0$ and by vector triple product rule $\nabla\times\mathbf{V}\times\zeta=(\nabla\cdot\zeta)\mathbf{V}-(\nabla\cdot\mathbf{V})\zeta$. The vorticity flux of the flow changes with time assuming non-divergence of vorticity without losing generality and using anelastic approximation (Jung and Arakawa 2007) under the combined effect of five processes that can be represented as:

$$\frac{\partial\zeta}{\partial t}=-(\mathbf{V}\cdot\nabla)\zeta_a+(\zeta_a\cdot\nabla)\mathbf{V}-\zeta_a(\nabla\cdot\mathbf{V})$$
$$+\frac{\nabla\rho\times\nabla p}{\rho^2}+\nabla\times\mathbf{F},\qquad(2)$$

where ζ is the relative vorticity; $\zeta_a=\zeta+2\Omega$ is the absolute vorticity; Ω is the Coriolis parameter. The left-hand side represents the local time tendency of

ζ. The first term on the right-hand side represents the advection of ζ_a at a certain point by the flow itself. The second term represents stretching or compression of the vortex, which passes through a certain point. It arises from the spatial variation of the velocity field in the direction of the vortex tube. The third term gives the three-dimensional convergence or divergence at that point. It reflects the mass redistribution of the flow due to the conservation of angular momentum. The fourth term of the right-hand side of the equation is the tilting term which comes from the baroclinicity. The last term represents the effect of friction and other subgrid-scale processes on the vortex passing through the point. The modified form of the vertical vorticity equation, including the forcing of diabatic heating, was discussed by Wu and Juan (2001). However, a recent study by Wang *et al.* (2016) obtained a similar form of the equation as equation (2) with the assumption that the change in density and horizontal gradient of entropy have been represented in the last term on the right-hand side of equation (2).

- Diabatic heating increases in the TC core region due to condensation and microphysical processes. We have represented the diabatic heating by material change of rate of potential temperature θ following Smith and Montgomery (2016), Rajasree *et al.* (2016a, b); Sheng *et al.* (2021) and Xie *et al.* (2021), i.e., total 3-dimensional derivatives of potential temperature given by the formula $\dot{\theta} = \frac{\partial\theta}{\partial t} + (\mathbf{V} \cdot \nabla)\theta$, where θ is the potential temperature, and $\mathbf{V}$ is the wind velocity.
- Okubo–Weiss (OW) parameter measures the balance between vorticity and deformation. It is defined as $\mathrm{OW} = \boldsymbol{\zeta}^2 - {S_1}^2 - {S_2}^2$, where $\zeta = \frac{\delta v}{\delta x} - \frac{\delta u}{\delta y}$ is the relative vorticity, $S_1 = \frac{\delta u}{\delta x} - \frac{\delta v}{\delta y}$; normal component of strain, i.e., stretching component, and $S_2 = \frac{\delta v}{\delta x} + \frac{\delta u}{\delta y}$; shear component. Therefore, a positive value of the OW parameter indicates the favourable region for rotation, and that of the negative value means strain-dominated, i.e., unfavourable region.
- Baroclinicity has been calculated using the formula $(\frac{\nabla p \times \nabla \rho}{\rho^2})$. The baroclinicity is developed in the inner core of TCs due to latent heat release from the condensation of water vapour. The increase in the baroclinic instability at the middle tropospheric environment of the TC core causes the strengthening of lower-level convergence and thereby the spin-up.
- Moisture flux in the vertical direction: The vertical gradient of moisture flux has been calculated from the high-resolution analysis using the formula: $VMF = (\frac{\partial wq}{\partial z})$, where w is vertical velocity and q represents the specific humidity of water vapour.

The understanding based on the analysis of these parameters has been presented in the next section.

3. Results and discussions

The NIO basin differs from its Atlantic or Pacific counterparts as it is warmer and shallower, resulting in the environmental factors dominating in deciding the TC behaviour (Bhalachandran *et al.* 2019). Therefore, the analysis focuses on how the environmental factors control the local environments within the vortex that favour the growth and maintenance of the TC core convection. The following section investigates the TC inner core vortex evolution, asymmetric–axisymmetric structure, CAPE, relative vorticity evolution, vertical velocity, RI, warm-core formation and strengthening (intensification), and deformation *vs.* rotation during the life cycle of TCs Fani (2019), Luban (2018), and Ockhi (2017) formed over NIO.

3.1 *CAPE and Azimuthally averaged vortex spin-up evolution*

Williams and Renno (1993) analysed CAPE variation in TCs lifespan and indicated that CAPE value above 1000 Jkg^{-1} favours buoyant updrafts. The temporal evolution of CAPE averaged over the 2°×2° area about the TC centre is shown in figure 2(a–c). The analysis indicates that CAPE values more than 1000 Jkg^{-1} since 48 hrs before cyclogenesis and during their lifespan ensured the thermodynamic favourability to develop a buoyant updraft. For TC Fani, large values of CAPE (above 1000 Jkg^{-1}) were prevailing in the neighbourhood of the TC centre for 48 hrs before cyclogenesis. For TC Luban, a well-built CAPE is observed about 24 hrs from the genesis stage. Finally, for TC Ockhi, a very strong CAPE (above 1200 Jkg^{-1}) has been prominent since 48 hrs before cyclogenesis. Strong CAPE was present at the boundary layer (BL) of TCs. The BL CAPE is found to be in the range of 1400–1600 Jkg^{-1} throughout the life of all the TCs.

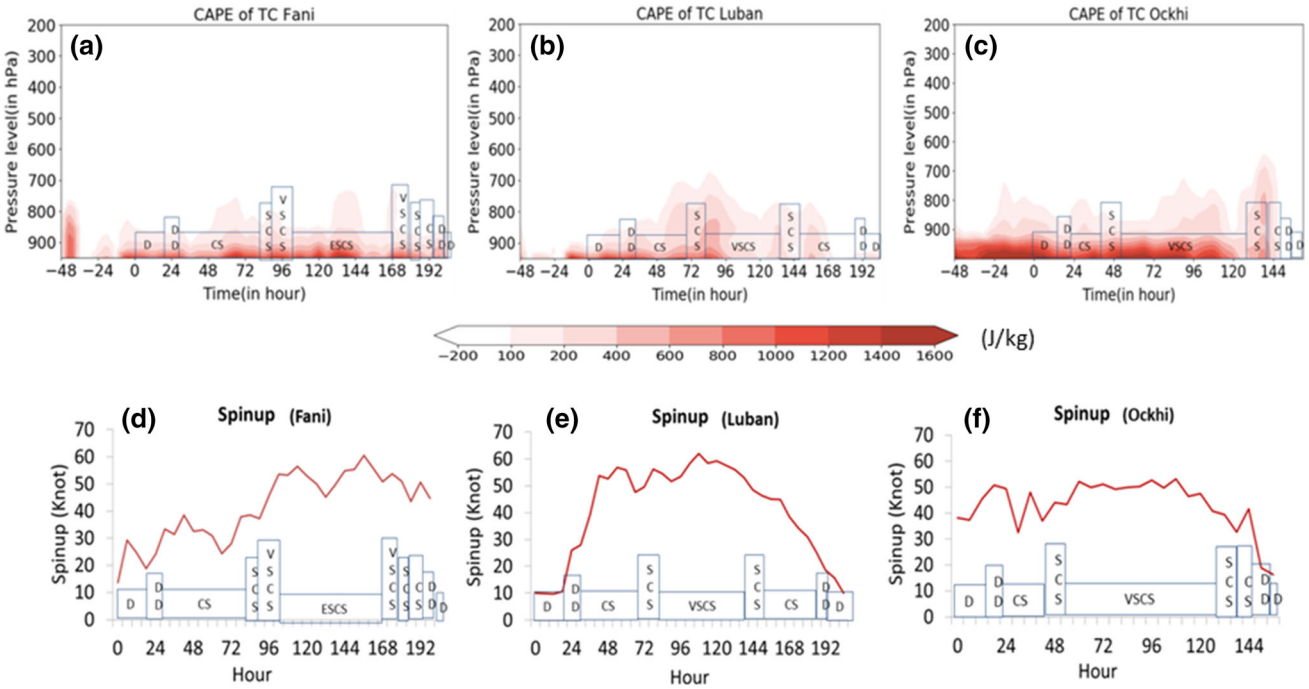

Figure 2. Time evolution of CAPE of TC **(a)** Fani, **(b)** Luban, and **(c)** Ockhi. Time series of the azimuthal-mean maximum tangential wind component or spin-up in knots of TC **(d)** Fani, **(e)** Luban, and **(f)** Ockhi at 850 hPa.

The sizes of the tropical cyclone based on the vorticity approach represent the outer radius of the cyclone beyond which no presence of deep convection is assumed (Jaiswal *et al.* 2019). These radii of the analysed three cyclones have been observed within 350 km while studying different quadrant radii in their life cycle (discussed later; section 3.7). For the calculation of spin-up, we studied the evolution of strong-deep convection and weak convection surrounding primary circulation up to $\sim 5^{\circ}$ area from the TC centre. Further, the radial increments of about 36 km ($\sim 0.3^{\circ}$) from the centre of the TC have been used for obtaining nearly smooth variation of averaged maximum spin-up (in 36 km) as the changes of their magnitudes in the 36 km do not deviate much.

In figure 2, the second row shows the time series of the azimuthal-mean maximum tangential wind component (spin-up) at 850 hPa for TCs (d) Fani, (e) Luban, and (f) Ockhi. TC Fani shows a gradual increment in spin-up up to the extremely severe cyclonic storm (ESCS) stage with a maximum spin-up of 60 knots. In the case of TC Luban, the rapid growth of spin-up was seen at the cyclonic storm stage and showed a maximum spin-up of 60 knots at the very severe cyclonic storm (VSCS) stage. Spin-up of TC Ockhi reclines between 30 and 50 knots from depression (genesis) to the dissipation stage. From figure 2, it is clear that the evolution of azimuthal-mean maximum wind is strongly correlated to the distribution of CAPE.

In a cyclogenesis environment, sufficient CAPE and cyclonic ζ at the lower level should exist (Montgomery *et al.* 2006). During cyclogenesis, moisture and heat transfer (through evaporation) generates CAPE from the underlying sea surface. Enhanced CAPE indicates that higher total column water implies fewer convective downdrafts. In addition, the systems with a higher convergence in the low level help strengthen the BL tangential wind. Therefore, the higher spin-up could support RI onset once the TC experiences higher CAPE in its lifetime. In addition, it warms the BL due to enhanced evaporation and wind-induced heat exchange, which further enhances the CAPE. This process helps in strengthening the vertical velocity of the convective vortices region in the bottom-up mechanism described by Montgomery *et al.* (2006) and Bell and Montgomery (2010). The CAPE generated in this process is released when moist air convects in the eyewall, condenses, and precipitates. Thus, ocean heat energy is transformed to CAPE, converted to potential energy, and finally, into the storm kinetic energy (Lee and Frisius 2018).

3.2 *Relative vorticity evolution*

Vortex stretching plays a vital role in the development and amplification of turbulence. Stronger localised vorticity near the core of the circulation corresponds to a more intense TC (Ditchek *et al.*

2017). ζ at 850 hPa is the dominant environmental factor affecting TCs' intensification (Wu *et al.* 2020). There is a strong correlation between the initial disturbances and high ζ values at the surface (Gray 1968). There are two mechanisms proposed in the literature for the evolution of relative vorticity. Bister and Emanuel (1998) proposed the first mechanism, and after that, it was applied to study TC evolution by many investigators (e.g., Kutty and Gohil 2017). This mechanism hypothesises that the vortex formation in the genesis period's mid-troposphere is influential and is popularly known as the top-down approach. The second approach for the cyclogenesis and evolution of TC is the bottom-up mechanism. This approach was proposed by Hendricks *et al.* (2004), Montgomery *et al.* (2006), and Wang (2012) and successfully applied for studying the evolution of the TCs over different parts of the oceanic basins (Rajasree *et al.* 2016a, b). The ζ intensification occurs from the lower troposphere to the upper troposphere with the intensification of the TCs, and the column height of TC decreases with the dissipation of the TCs. Dunkerton *et al.* (2009) and Gjorgjievska and Raymond (2014) noted that both approaches are not exclusive but are complementary and exist on a different scale. The top-down mechanism was observed over the meso-α scale, and the bottom-up mechanism was observed over the meso-β scale as a part of the turbulent cascade during the TC intensification.

Figure 3 illustrates the vertical cross-section ζ of TC Fani (first row), Luban (second row), and Ockhi (third row) during the RI and MI stage. As evident from the figure, the bottom-up mechanism at meso-β scale prominently contributes to the organisation and deepening of rotation (vorticity) around the centre of the vortex. According to the marsupial paradigm (Dunkerton *et al.* 2009), the quasi-Lagrangian cyclonic circulation protects the rotation-dominating region from the shear-dominating surrounding. Stretching of the vortex in terms of magnitude and structure is contributed by the interaction of cyclonic rotation and deep convection. The vertical stretching of the vortex has been observed with the intensification of these TCs.

During RI of TC Fani (12 UTC 29 Apr to 12 UTC 30 Apr 2019), the ζ intensified from 20–30 $\times$ 10^{-4} to $> 40 \times 10^{-4}$ s^{-1}, and the vortex column was extended from middle to upper troposphere (figure 3a, b). The increment in ζ in the lower troposphere for TC Luban RI (06 UTC 09 Oct to 06 UTC 10 Oct 2018) is from 10–20 $\times$ 10^{-4} to 20–30 $\times$ 10^{-4} s^{-1}, and the vortices became more organised and stretched up to upper troposphere (figure 3d, e). In the RI period of TC Ockhi (06 UTC 29 Nov to 06 UTC 30 Nov 2017, and 00 UTC 01 Dec to 00 UTC 02 Dec 2017) at the genesis period, when the TC intensified from depression to cyclonic storm (CS) stage within 24 hrs, ζ increased from 10–20 $\times$ 10^{-4} to 20–30 $\times$ 10^{-4} s^{-1} (figure 3f, g). Therefore, as seen from the figures, the intensification of ζ is about 15–20 $\times$ 10^{-4} s^{-1} during RI of the three TCs and vortex column extended from middle to the upper troposphere and became well organised in 24 hrs. At the MI stage of TC Fani, a well-firmed vortex column throughout the tropospheric column with ζ value above 40 $\times$ 10^{-4} s^{-1} (figure 3c) is observed when it was in ESCS. The axisymmetric convective ring model (Willoughby 1979; Shapiro and Willoughby 1982) for the intensification of TCs suggests that the magnitude of ζ is inversely related to the vortex structure's spatial span.

3.3 *Vorticity budget and fluxes*

The vorticity budget has been estimated based on the high-resolution mesoscale analysis to understand the development and evolution of convection inside the TC. The vorticity budget has been calculated using equation (1) for the region of size 2° $\times$ 2° around the centre of TC for every 6 hrs. The calculated magnitudes of six terms in equation (2) have been shown in figures 4–6 for three TCs.

Wang (2012) indicated that the location of meso-β scale relative vorticity is maximum at 600 and 700 hPa. However, the present case study shows that for TC Fani, the relative vorticity tendency is higher throughout the tropospheric layers from 48 hrs (after convention strengthens due to vortex stretching, as seen from figure 4c) till 110 hrs. Fani underwent RI since 84–108 hrs. The systems Luban and Ockhi show different vertical growth (figures 5a and 6a) since 24 hrs and genesis due to dominant advection of vorticity in lower and middle troposphere (figures 5b, 6b). For TC Luban, the relative vorticity maxima are observed between the surface to 750 hPa just before attaining the RI (figure 5a). On the other hand, Ockhi shows the prominently high vorticity tendency up to the mid-tropospheric region till 72 hrs, promoting two RI phases in its lifetime (figure 6a). However, the increase in surface spin-up is not only because of

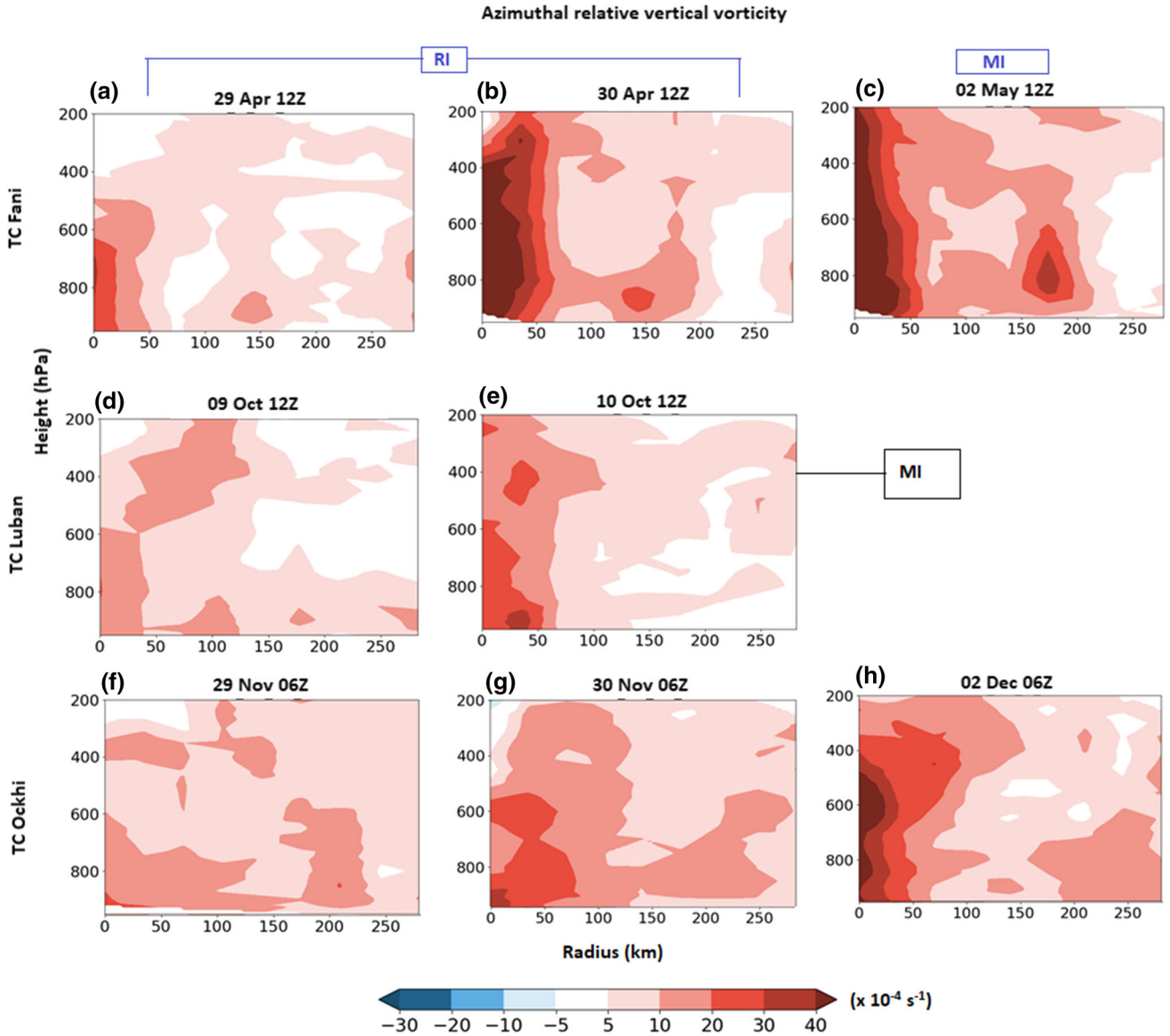

Figure 3. Azimuthal cross-section of ζ of TC Fani (first row), Luban (second row), and Ockhi (third row) at RI and MI stage. MI of TC Luban happened immediately at the end of RI.

the increased mid-tropospheric vorticity proposed by Wang (2012). Moreover, the high meso-β scale relative vorticity maximum in the case of Luban was due to the increase in surface-level convergence (RI: 78–102 hrs; figure 5d) also agrees well with Wang *et al.* (2010) and Mohanty *et al.* (2021). The magnitude of baroclinicity (figures 4e, 5e, and 6e) for TC Fani, Luban, and Ockhi ranged from 100 to 400 $\times$ 10^{-9} s^{-2}, the highest for Ockhi.

The advective vorticity flux term shows a positive tendency in the middle to upper troposphere, mostly over 750 hPa for Fani, and is positive over 850 hPa for Luban and Ockhi (figures 4b, 5b, and 6b). At the same time, the lower troposphere is mostly dominated by negative frictional and other subgrid-scale processes at the core of the system below 650 hPa for all three systems at the meso-β scale. Therefore, it can be inferred that the upper-level positive advection of vorticity is the major contributor to the high net positive vorticity that made the condition more favourable for the system to undergo RI. The convergence at the lower level is high enough, i.e., higher than 120 $\times$ 10^{-9} s^{-2} for Fani and 100 $\times$ 10^{-9} s^{-2} for Ockhi in the BL during the RI phases of the systems. For TC Luban, the convergence was comparatively less $\sim$30 $\times$ 10^{-9} s^{-2}. The strong BL convergence offsets the frictional spindown for all the three systems considered, helping the system to build up strong intensity quickly. Wang (2012) and Mapes and

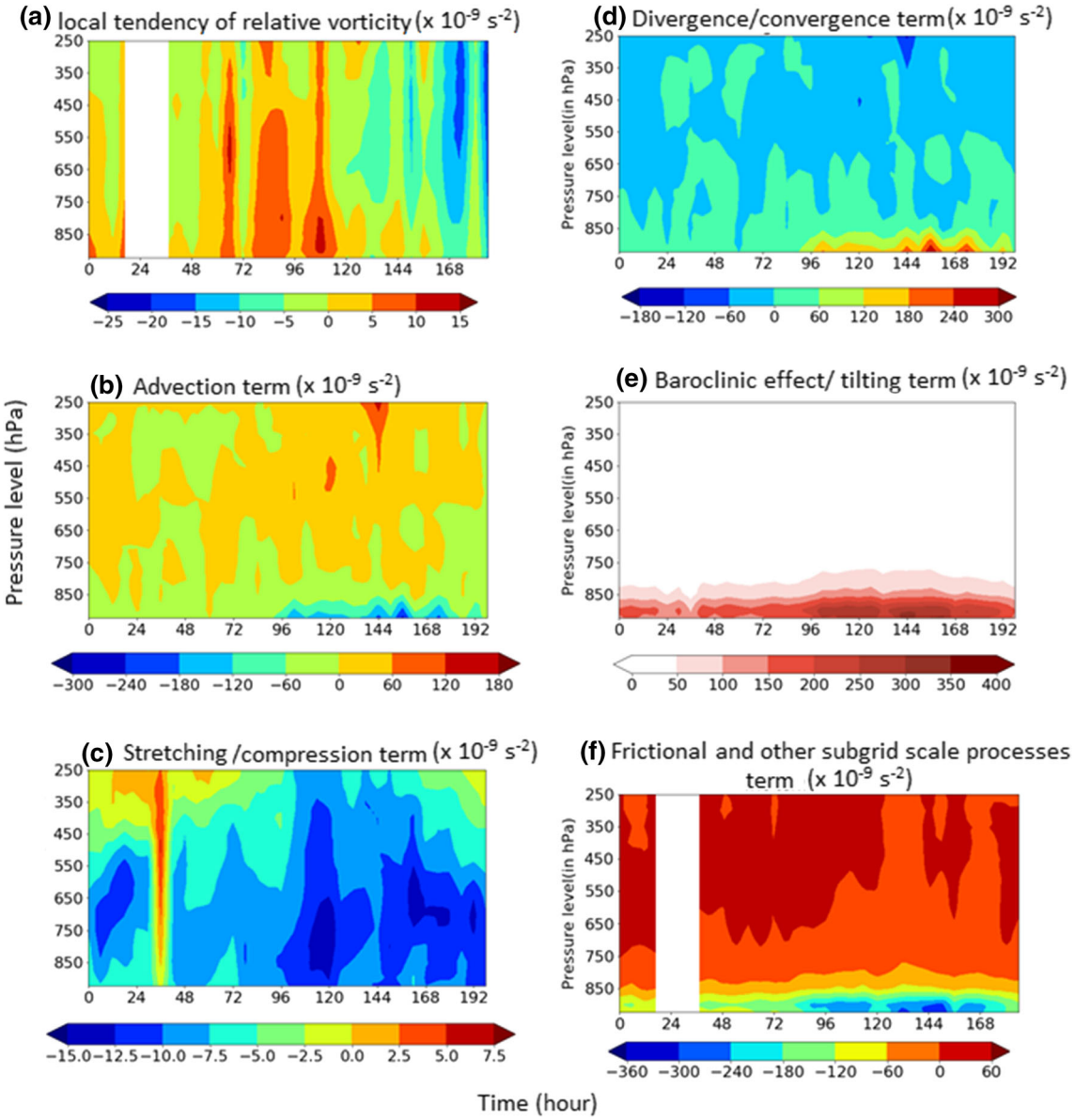

Figure 4. Vorticity budget at the TC Fani region (2° × 2° area around the centre) during its life span where the terms represented are **(a)** local tendency of relative vorticity, **(b)** advection term, **(c)** stretching term, **(d)** divergence/convergence term, **(e)** baroclinic effect, and **(f)** frictional and subgrid-scale processes.

Houze (1995) suggested that the enhanced low-level convergence and upper-level divergence are associated with convective precipitation, and the middle-level convergence and divergence show the presence of stratiform clouds. During the process of RI, the heat release from these convective systems gives positive feedback for further intensification.

3.4 *Warm core formation and strengthening*

Condensation of the mid-tropospheric moisture causes diabatic heating, leading to increased convections and forms VHTs (Montgomery *et al.* 2006). Figure 7(a–c) shows the temporal evolution of the vertical distribution of diabatic heating (first row) taken as the areal maximum over 2° × 2° from the TC centre of TC Fani (a), Luban (b), and Ockhi (c). An increase in the diabatic heating (above 30 Kh^{-1}) throughout the column has been seen 24 hrs before cyclogenesis. It is correlated with the moistening of the middle troposphere about 24 hrs before cyclogenesis (refer to figures 10a, 12a, 14a). The latent heat released during condensation processes further strengthened the vortex. The increment in the vertical velocity has been observed 24 hrs before the dissipation stage for TC Fani (figure 7d) and from the dissipation for TC Luban and Ockhi (figure 7e and f). RI of TC is

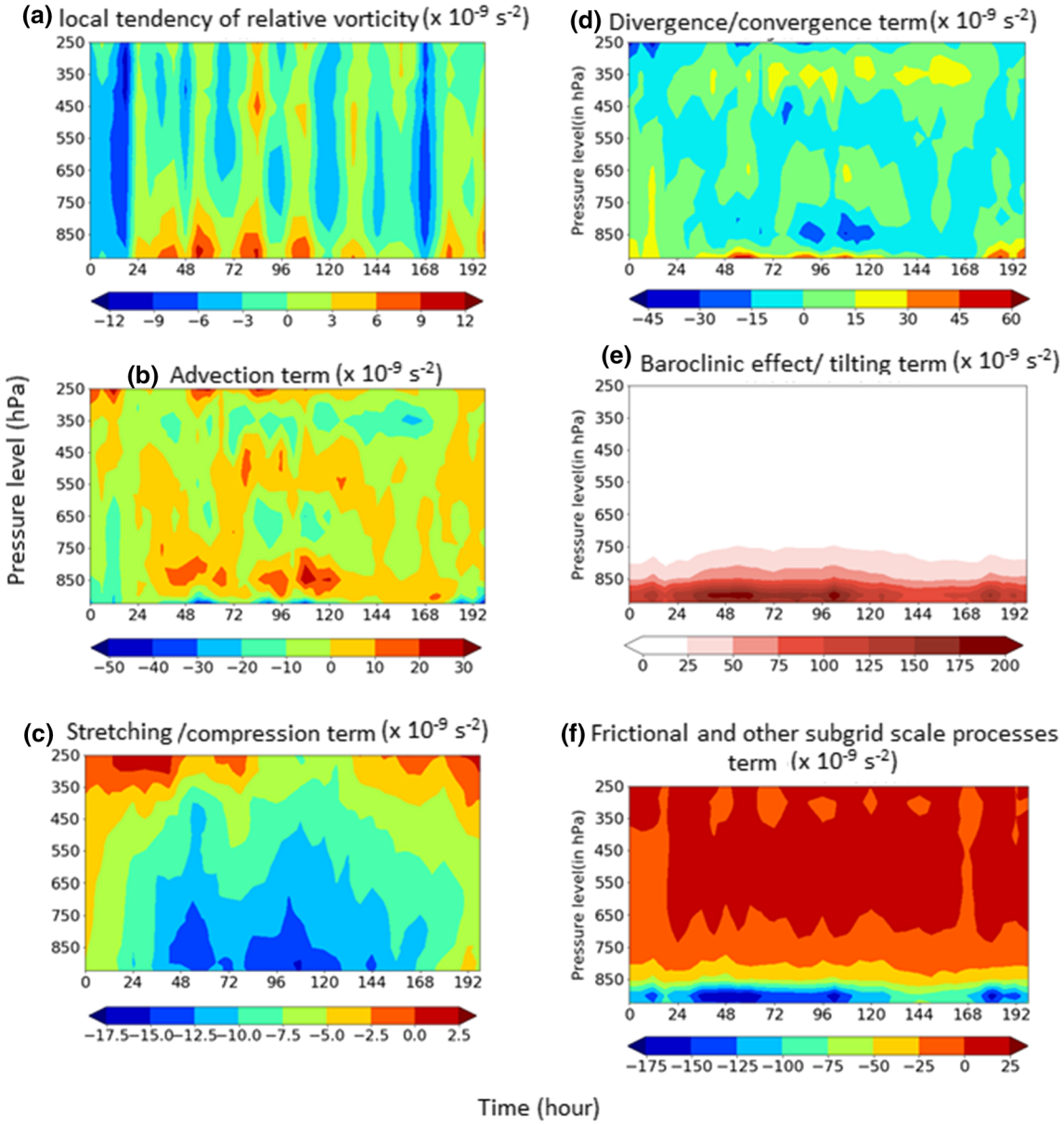

Figure 5. Vorticity budget at the TC Luban region (2°× 2° area around the centre) during its life span where the terms represented are **(a)** local tendency of relative vorticity, **(b)** advection term, **(c)** stretching term, **(d)** divergence/convergence term, **(e)** baroclinic effect, and **(f)** frictional and subgrid-scale processes.

associated with strengthening the vortex, causing intense deep convection, which leads to 'more efficient' diabatic heating (Hack and Schubert 1986; Vigh and Schubert 2009). A rapid growth in the diabatic heating rate is observed when TCs experienced RI (around 84th hr for TC Fani, 66th hr for Luban, and 42nd hr for Ockhi). The consequent increase in vertical velocity (above 0.2 ms^{-1}) at the upper troposphere (figure 7d–f: second row) due to diabatic heating contributes to maintain the column tower of TC.

Figure 7(g–i) shows that the sharp increase in the moisture's vertical transport was observed a few hours before TCs intensified to the MI stage. In our companion paper (Munsi *et al.* 2021), we have discussed that the externally forced convergence conditions were responsible for the TCs to intensify to their MI stages. The cyclonic circulation of TC Fani was embedded in between the anticyclonic circulations in the south and north regions. It caused an increase in the lower level confluence at the downwind right quadrant of the TC, which forced it to the MI stage.

TC Luban reached to MI stage due to a sudden increase in the upper air divergence. TC Ockhi reached to MI stage due to increased lower level

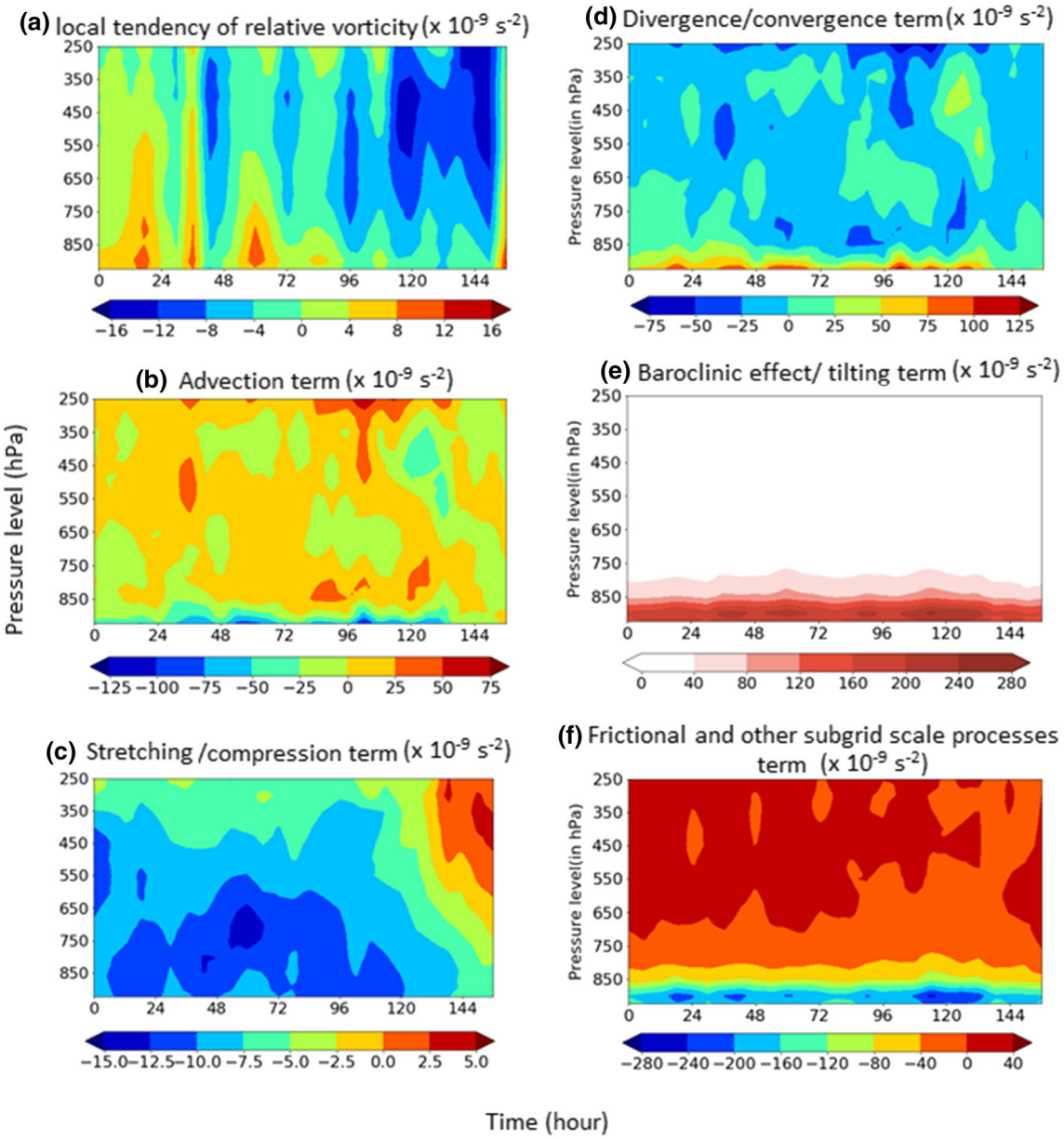

Figure 6. Vorticity budget at the TC Ockhi region (2°× 2° area around the centre) during its life span where the terms represented are **(a)** local tendency of relative vorticity, **(b)** advection term, **(c)** stretching term, **(d)** divergence/convergence term, **(e)** baroclinic effect, and **(f)** frictional and subgrid-scale processes.

convergence under the influence of ridgeline in its north direction (shown in our companion paper; Munsi *et al.* 2021). These external forces caused an increment in the microphysical processes associated with warm-core strengthening and a sudden rise in the vertical transport of moisture (as seen in figure 7a–c and g–i). The increase in the vertical moisture flux for TCs Fani and Ockhi was up to 21×10^{-5} kg kg^{-1} s^{-1} and that for TC Luban was 12×10^{-5} kg kg^{-1} s^{-1}. The positive feedback of diabatic heating, high baroclinic instability, increase in the vertical velocity, and further vertical moisture transport causes the continuous strengthening of inner-core convection and the intensification of TCs.

In the TC disturbance, the baroclinicity developed due to latent heating in the warm core region. Also, the moisture flux from the ocean causes a decrease in the density of the lower troposphere. As a result, it causes an increase in the potential instability, causing the inner core environment to be more buoyant. This environment generates buoyant updrafts with large values of vertical velocity. The increase in the vertical velocity drives the vertical moisture transport, and their collocated increments have been observed (figure 7).

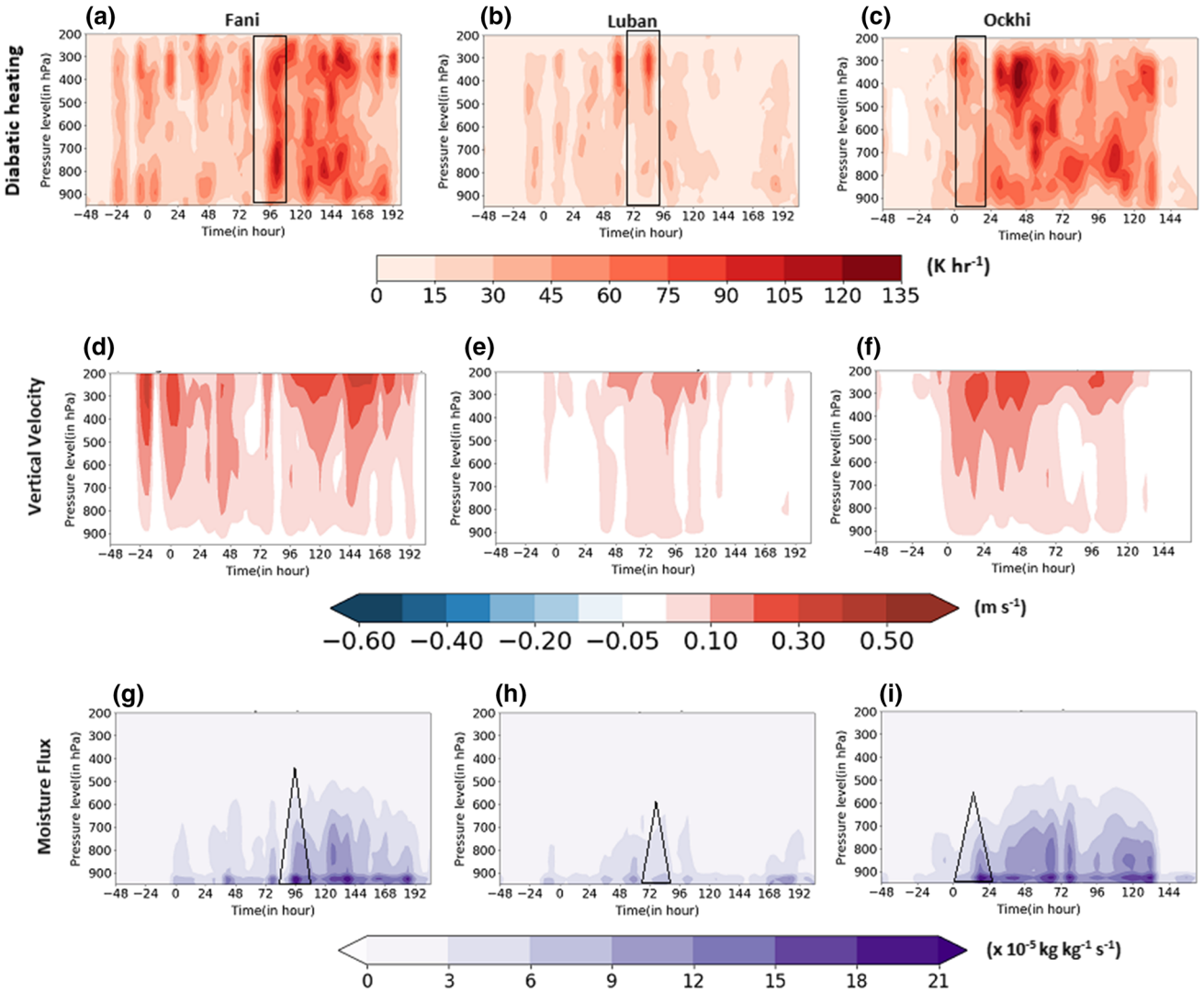

Figure 7. Temporal evolution of the rate of diabatic heating (first row) in Khr^{-1} taken a maximum of 2° × 2° latitude × longitude area around TC centre of TC Fani **(a)**, Luban **(b)**, and Ockhi **(c)**. Vertical velocity (second row) in ms^{-1} of TC Fani **(d)**, Luban **(e)** and Ockhi **(f)**; moisture flux (third row) in kg kg^{-1} s^{-1} of TC Fani **(g)**, Luban **(h)**, and Ockhi **(i)** taken an areal average of 2° × 2° latitude × longitude over TC centre.

3.5 *RI dynamics*

The complex ocean–atmospheric interaction of troposphere and ocean decides the direction of propagation of the TCs. Environmental steering flow controls the propagation of TC with multiple physical mechanisms operating simultaneously (Carr III and Elsberry 1990). TCs moved in the direction determined by β gyre (Carr III and Elsberry 1990; Ito *et al.* 2020), ocean surface warming (Sun *et al.* 2017) diabatic heating (Ito *et al.* 2020), horizontal and vertical structure (Ito *et al.* 2020), the strength of winds in TC radial band (Chan 1985; Carr III and Elsberry 1990) and vorticity gradient (Carr III and Elsberry 1990). Several mechanisms have been suggested for the understanding of RI processes. Molinari and Vollaro (2010) discussed the mechanism of how a sheared storm can undergo RI. High mid-tropospheric RH is a dominant factor for RI and maximum intensity arrival (Emanuel *et al.* 2004; Hendricks *et al.* 2010; Wu *et al.* 2012). Miyamoto and Takemi (2015) showed that larger values of the Rossby number trigger the RI of TCs. Geetha and Balachandran (2016) discussed the role of diabatic heating during RI of TC over NIO. Yan *et al.* (2019) showed that monsoon gyre mechanisms affect the RI of TCs. Zhang *et al.* (2019) have shown that when mean kinetic energy is converted into eddy kinetic energy, an increase in the diabatic heating cause the RI of TCs. Our companion paper, Munsi

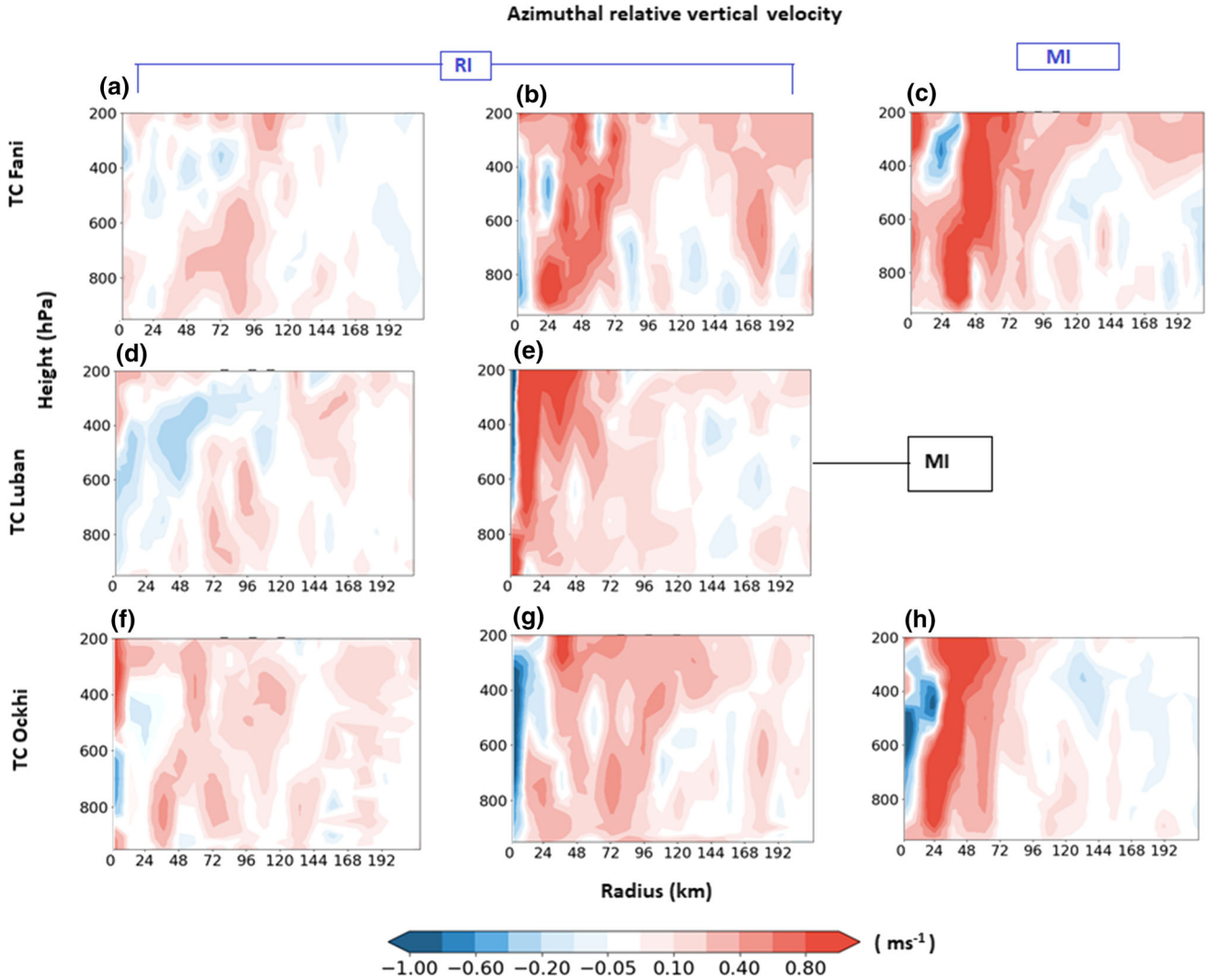

Figure 8. Azimuthal cross-section of the vertical velocity of TC Fani (first row), Luban (second row), and Ockhi (third row) at RI and MI stage.

et al. (2021), showed that high-resolution mesoscale analysis for these TCs simulated the RI appropriately. Stronger vertical motion in the inner radii region and a stronger radial gradient of vorticity is associated with increased outflow (Ditchek *et al.* 2017). Therefore, the azimuthal distribution of vertical velocity during RI and MI of TCs Fani, Luban, and Ockhi has been investigated in the next subsection.

3.5.1 *Vertical velocity evolution*

When the increment in vertical velocity coincides with the increase of relative vorticity, the association becomes dominant in the convective system. It has been observed from figure 8 that the vertical velocity at the lower to upper troposphere strengthened from 0.2 to 1 ms^{-1} during the RI stage of TC Fani (figure 8a, b) and Luban (figure 8d, e). During the RI stage of TC Ockhi, vertical velocity was observed from 0.2 to 0.8 ms^{-1} (figure 8f, g). The unorganised, weak, discontinuous vertical columns became organised around the eye with intense vertical velocity throughout the column after RI. In the case of TC Ockhi, after RI, the whole column has not been seen as strong as Fani or Luban, as it showed RI at the genesis phase. After RI, TC Fani and Luban were in ESCS and VSCS stage, respectively, whereas Ockhi was in the CS stage. At the MI stage, the maximum vertical velocity was above 1 ms^{-1} for all three TCs (figure 8c, e, and h). Thus, it is coagulated with strengthening these TCs during RI and MI. Strong downward vertical velocity at the eye region has been observed. Radially outward extension of strong vertical velocity at the upper level is seen

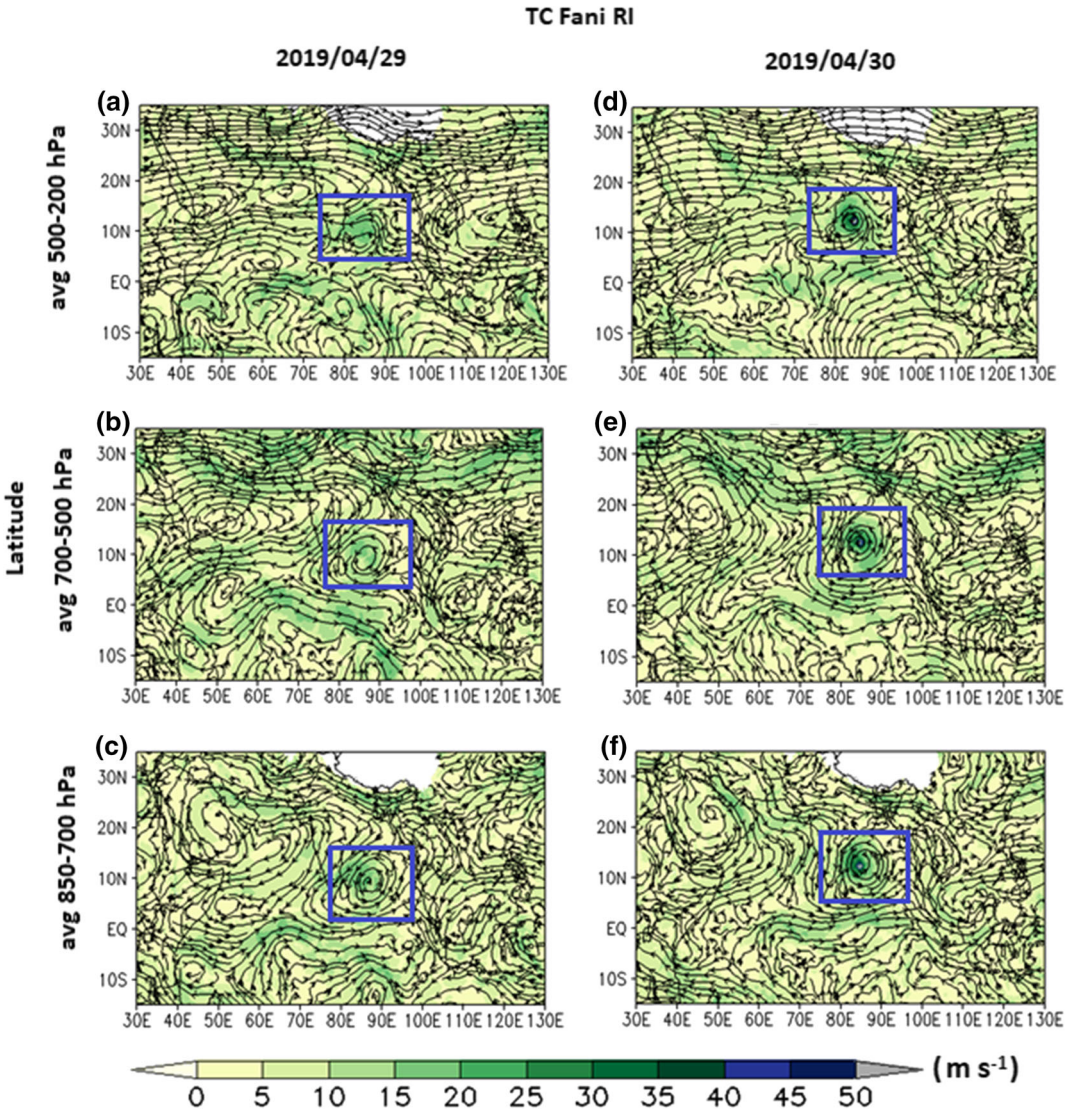

Figure 9. Upper, middle, and lower tropospheric circulation (streamlines) during the RI stage of TC Fani. The shaded background indicates the wind speed (m s^{-1}).

due to upper tropospheric outward radial flow and middle to lower tropospheric inward radial flow (Montgomery *et al.* 2006).

3.5.2 *Temporal variation of environmental features and environmental steering flow*

The large environmental circulations which influence the TC inner core dynamics have been analysed in this section. Figure 9 shows the lower, middle, and upper tropospheric circulation during the RI stage of TC Fani. During the RI of TC Fani initiation, the anticyclonic circulation extending from lower to upper troposphere was present over the Arabian Sea, south India, and the Myanmar–Indonesian region. The TC Fani was embedded in two anticyclonic circulations (figure 9). Anticyclonic circulations at the north of the TC were not conducive for its intensification. The cyclonic circulation of TC Fani was extended up to the middle troposphere (figure 9a–c). The Inter-Tropical Convergence Zone (ITCZ) was located about 10°S of the equator. At this period, TC Fani was located in the region with warm SST (29–31°C, figure 7a). Under the influence of TC Fani, the part of ITCZ near the equatorial Indian Ocean migrated to the north of the equator providing moisture to the rain bands of TC Fani. It caused middle tropospheric relative humidity to saturate (>80%, figure 10a) at the core (1° × 1° region around the TC centre) of the TC. The consequent increase in the diabatic heating (∼30 Khr^{-1}, figure 10b) followed by the release of CAPE (∼1200 J kg^{-1}, figure 10c) causes the conversion of CAPE to

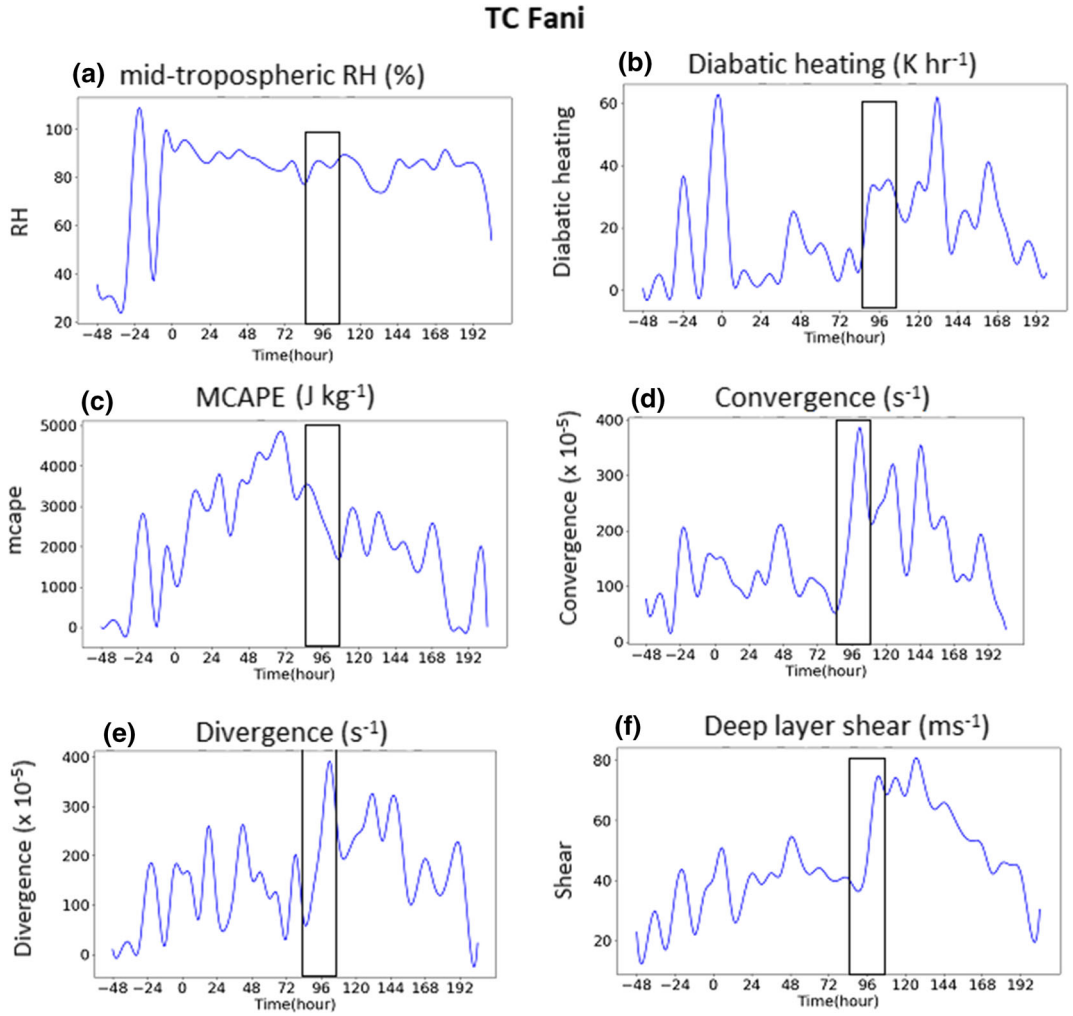

Figure 10. Mid-tropospheric (average of 700–500 mb) relative humidity (RH) averaged over 1° × 1° area about the centre of TC **(a)**, areal maximum of diabatic heating **(b)**, evolution of MCAPE at the centre of TC **(c)**, lower level (850 hPa) convergence **(d)**, upper level (200 hPa) divergence **(e)** and deep layer shear (DLS) **(f)** over 1° × 1° latitude × longitude area about the centre of TC Fani.

kinetic energy. It results in a sudden increase in the lower tropospheric convergence (figure 10d), i.e., an increase in moist surface inflow, upper tropospheric divergence (figure 10e), and deep layer wind shear (40–70 ms^{-1}, figure 10f). Thus, the migration of the equatorial IO portion of ITCZ to the north of the equator and the accumulation of moisture in the middle troposphere at the core fueled the TC. Notably, low-level convergence and upper-level divergence were maximum during the RI phase of TC Fani compared to that of the MI phase (144–165 hrs). The RI of TC Fani caused the cyclonic circulation to extend up to the upper troposphere (figure 9d–f) and the migration of anticyclonic circulation over the Saudi Arabian and Pacific oceans, which was conducive for northwestward migration and intensification.

In the case of TC Luban, cold and dry air intrusion from the north Indian landmass at the lower troposphere (figure 11c) and cyclonic circulation was extended to the middle troposphere (figure 11b–c). At the genesis phase, the MJO index was in phase 1 with an amplitude of more than 1. This thermodynamic condition continued until RI and MI, favouring the convective activity. The anticyclonic circulation was present in the northeast of the TC, and a subtropical westerly jet was located further north (figure 11a). TC Luban was located on the southwest Arabian Sea, and simultaneously TC Titli was located over central BoB. Therefore, a large amount of moisture over BoB, Indian landmass, and equatorial Indian Oceans was fetched by TC Titli. Both TCs were intensifying as a dynamo; however, as TC Titli fetched moisture, there was a decrease in the values of middle tropospheric relative humidity (figure 12a), lower level convergence (figure 12d),

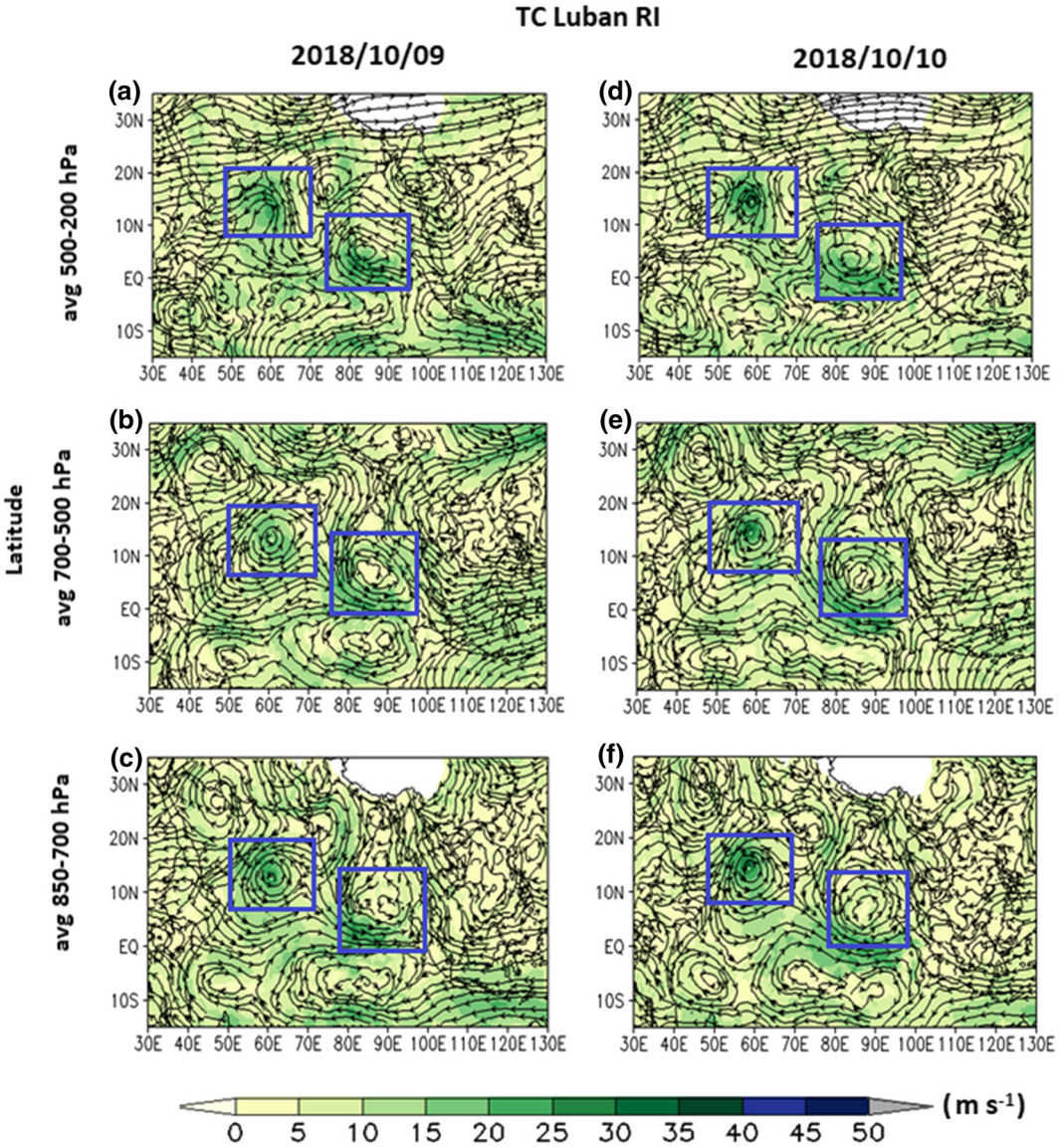

Figure 11. Upper, middle, and lower tropospheric circulation (streamlines) during the RI stage of TC Luban. The shaded background indicates the wind speed (ms^{-1}).

upper air divergence (figure 12e) before the RI stage. At 12–18 UTC 9 Oct 2028, TC Luban fetched moisture from the southeast Arabian Sea, off the Indian coast. It led to an increase in the middle tropospheric relative humidity (figure 12a), followed by rise in the diabatic heating ($\sim$30 K hr^{-1}, figure 12b) and release of CAPE (figure 12c). The release of CAPE led to converting available potential energy to kinetic energy. Hence, there was an increase in lower-level convergence (figure 12d), upper air divergence (figure 12e), and consequently, deep-layer shear (28 ms^{-1}, figure 12f). The RI causes the cyclonic circulation of TC Luban to extend up to the upper troposphere (figure 11d) and its northwestward migration (figure 11d–f).

TC Ockhi underwent two cycles of RI during its lifespan. During the first RI, it intensified to the CS stage from depression. During the second RI, it intensified from SCS to the VSCS stage. Before RI, the anticyclonic circulation was present in the middle (figure 13b) and upper troposphere (figure 13a) in the north of the TC. As a result, the cyclonic circulation of TC was extended up to the middle troposphere. An increase in the middle tropospheric relative humidity was observed during the first RI. Though there was a slight decrease in the relative humidity during the second RI, it was sufficient ($\sim$80%) to intensify the TC. The increase in diabatic heating (figure 14b) and release of CAPE (figure 14c) were observed in the case of both RI. The RI causes the cyclonic circulation of

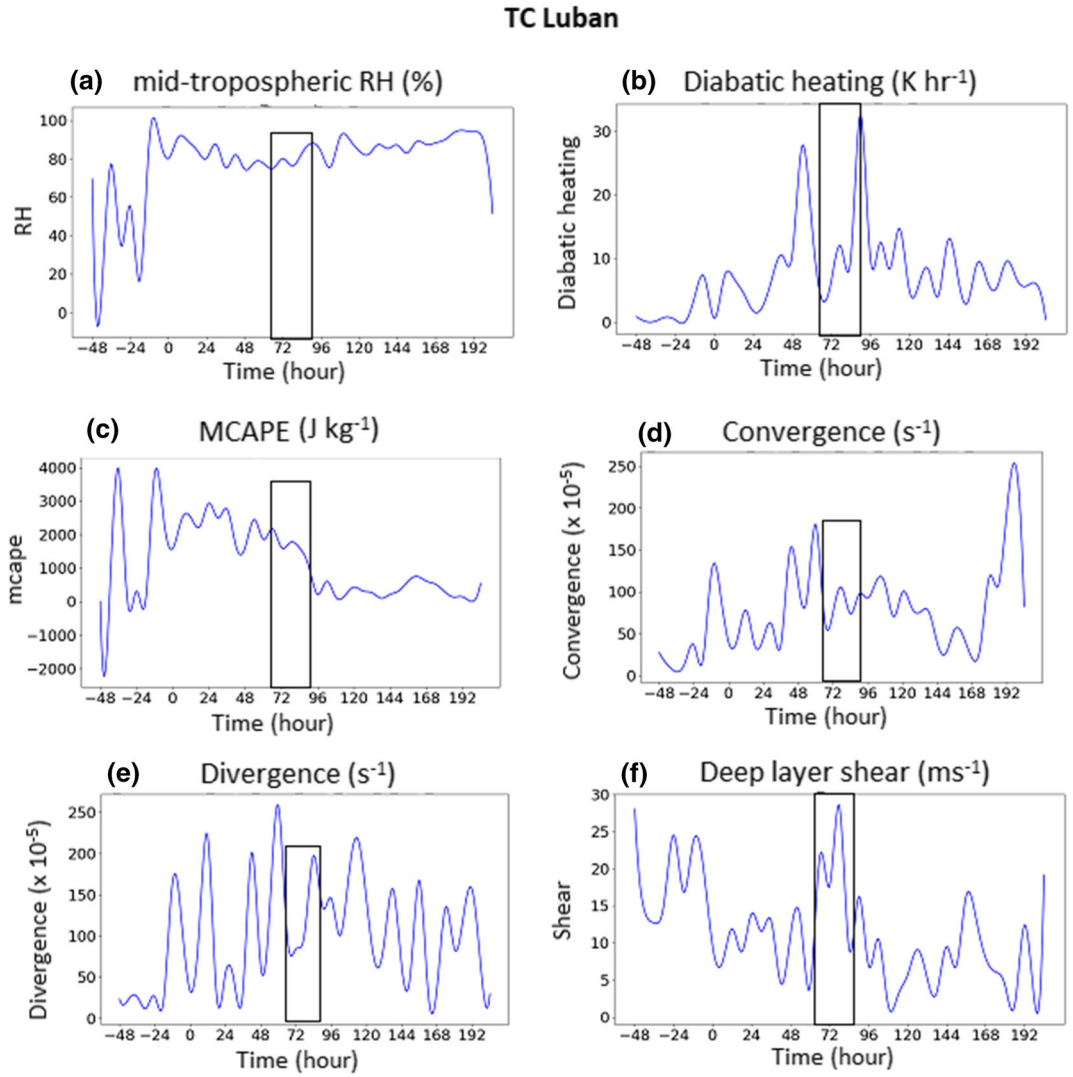

Figure 12. Mid-tropospheric (average of 700–500 mb) relative humidity (RH) averaged over 1° × 1° area about the centre of TC **(a)**, areal maximum of diabatic heating **(b)**, the evolution of MCAPE at the centre of TC **(c)**, lower level (850 hPa) convergence **(d)**, upper level (200 hPa) divergence **(e)** and DLS **(f)** over 1° × 1° latitude × longitude area about the centre of TC Luban.

TC to extend up to the upper troposphere (figure 13d). During the genesis period RI, the upper-level divergence has decreased. The reduction in the ventilation flow (at 200 hPa) may be caused by moisture accumulation in the vortex column. It helped in intense diabatic heating and led to second RI. A similar result of outward ventilation flow is at the upper troposphere above 300 hPa by storm related to northerly winds, have been shown by Chen *et al.* (2019). However, Sear and Velden (2014) showed that enhanced upper-level divergence in developing systems promotes ventilation in SW and NE quadrants adjacent to the core of the TC. Consequently, a reduction in the upper-level divergence causes a reduction in SW and NE directions from the centre of the system. However, the anticyclonic circulation at the north of TC Ockhi in the upper troposphere made the TCs northward propagation difficult immediately after the second RI. Thus, it further intensifies to a maximum intensity almost over the same region.

The temporal variation of deviation between the equivalent potential temperature between 950 and 750 hPa (θ_{ed}) for all the three TC cases has been analysed for their life cycle (figures not shown for brevity). The analysis indicated that the θ_{ed} for Fani remained almost constant from genesis to landfall. Luban shows a rising nature of θ_{ed} before RI, continuing till MI phase. However, Ockhi shows a rising θ_{ed} during the first RI phase and another peak during the second RI phase of the system. θ_{ed} is lying in the range of 14–17 $\times$ 10^{-5} K, the highest for Luban among all the three considered TC cases. The difference between the θ_{ed} for

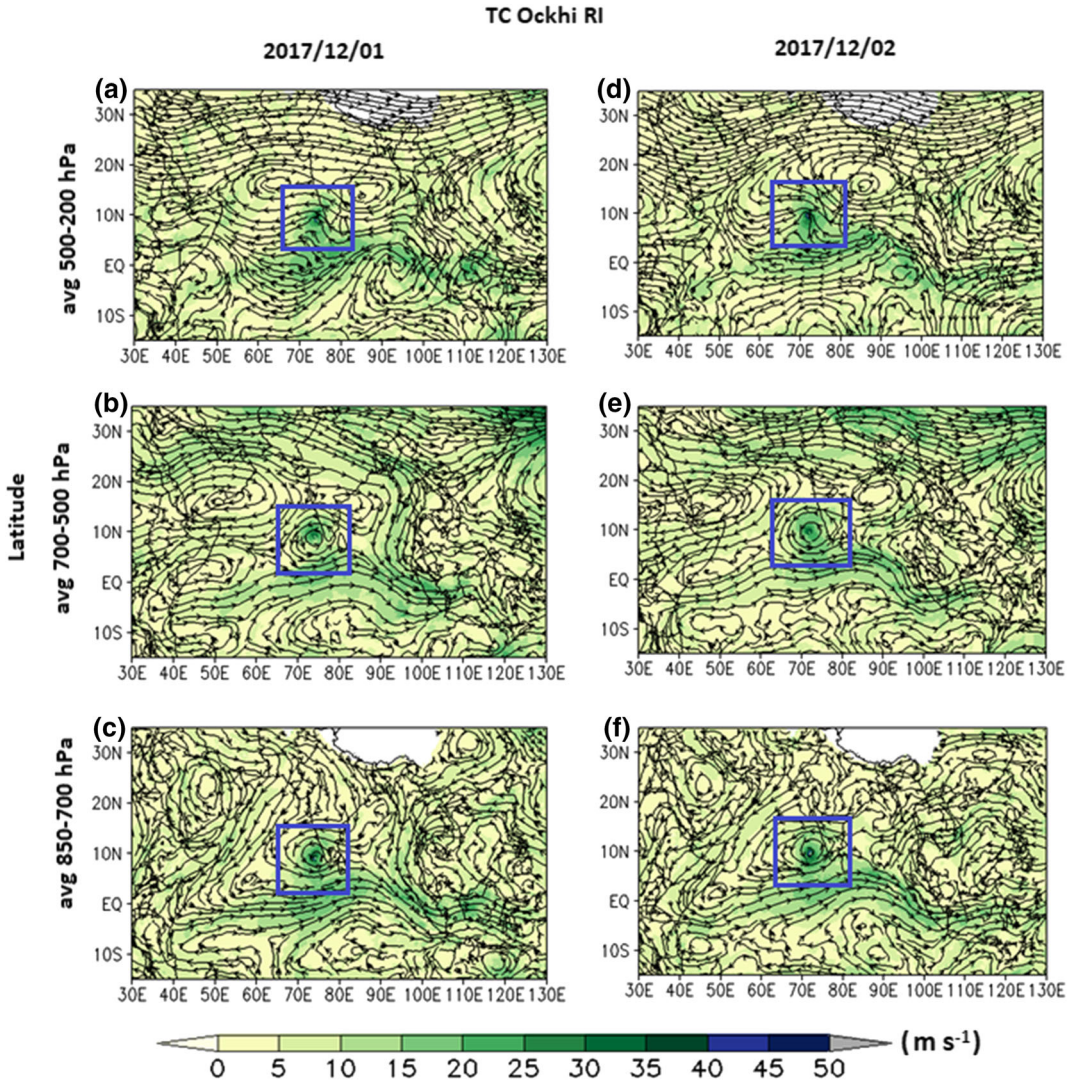

Figure 13. Upper, middle, and lower tropospheric circulation (streamlines) during the RI stage of TC Ockhi. The shaded background indicates the wind speed (ms^{-1}).

all three systems is mainly due to the moisture distribution in the β-scale region. The smaller temporal difference in θ_{ed} (1–2.5 K) for the TCs Fani, Luban, and Ockhi during their life cycle indicated that persistent convection over the core region, moistening of the middle troposphere, further elevating the values of middle-level θ_e, that reduces the downdraft convective available potential energy (Wang 2012). It provides a favourable environment to aid the convection process, creating the appropriate condition for the RI of the systems.

3.6 *Eyewall replacement cycle of TC Fani*

TC Fani (the other two cyclones did not go through the eyewall replacement cycle) underwent an eyewall replacement cycle after its MI stage and before its dissipation. The large-sized cyclone undergoes an eyewall replacement cycle when secondary maxima are developed in the convergence outside of the primary eyewall. Figure 15 depicts it in the INSAT3D images (Jaiswal *et al.* 2022). The azimuthal average of vertical vorticity from the mesoscale analysis also depicted the eyewall replacement cycle. The outer eyewall was formed outside the primary eyewall with secondary maxima of vertical vorticity on 18 UTC 1 May 2019. The secondary eyewall gradually contrasts radially towards the primary eyewall as we see the radius of the secondary eyewall decrease from 250 km to 150–200 km (figure 15h). However, after that, the eye of the TC Fani crossed the Odisha coast, and it started dissipating, which led to an increase in the size of TC Fani but weakened the vortex strength. The detailed mechanism of the eyewall

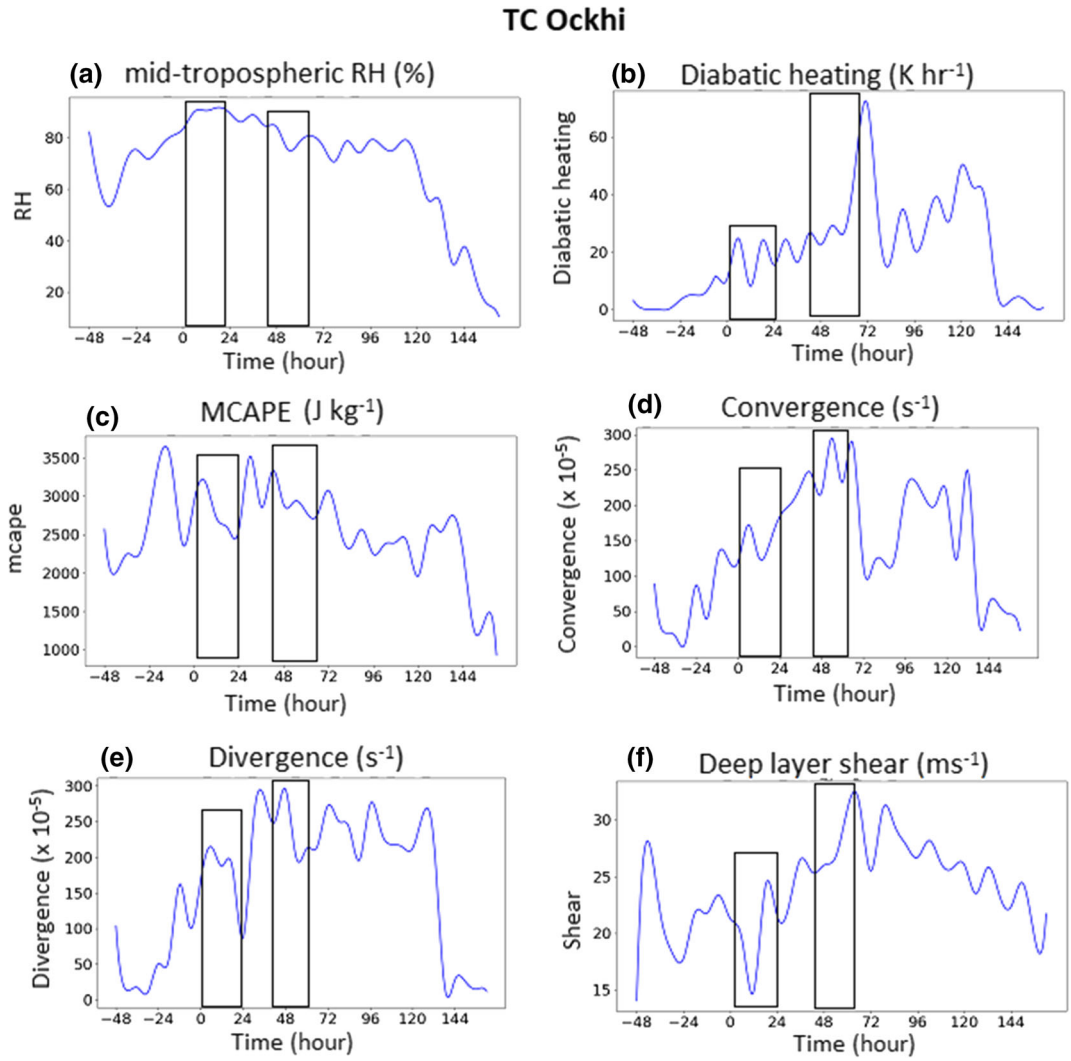

Figure 14. Mid-tropospheric (average of 700–500 mb) relative humidity (RH) averaged over 1° × 1° area about the centre of TC **(a)**, areal maximum of diabatic heating **(b)**, the evolution of MCAPE at the centre of TC **(c)**, lower level (850 hPa) convergence **(d)**, upper level (200 hPa) divergence **(e)** and DLS (f) over 1° × 1° latitude × longitude area about the centre of TC Ockhi.

replacement cycle requires further analysis, and we will carry it out in another article.

3.7 *Deformation vs. rotation and radii evolution*

The comparative influence of convection and deformation affects the temporal evolution of inner core formation during tropical cyclogenesis. Increasing vorticity is the signature of developed and enhancing convection, whereas the large shear value brings out deformation that resists forming the inner core column of deep convection. Thus the knowledge of the distribution of vorticity and deformation supports understanding the formation of deep convection. OW parameter helps us distinguish the flow into different regions: cyclonic rotation dominated region (OW is +ve) and deformation/strain dominated region (OW is –ve). A numerical experiment on two-dimensional turbulent flow leads to the segmentation of relative dominance of rotation and deformation (Elhmaidi *et al.* 1993). They observed a general eddy structure with an inner core dominated by vorticity with strain-dominated surroundings.

Furthermore, analysis of mesoscale eddies by the spatial distribution of the OW parameter is applied to distinguish vorticity-dominated eddy core from the surroundings, where, in general, deformation prevails. The evolution of the OW parameter calculated over an area of 4° × 4° (latitude × longitude) region about the centre of TC from genesis to mature stages is shown in figure 16 for TC Fani (first row), Luban (second row), and Ockhi (third row). Our analysis shows that the core region of TC gets a vorticity-dominated deep convective

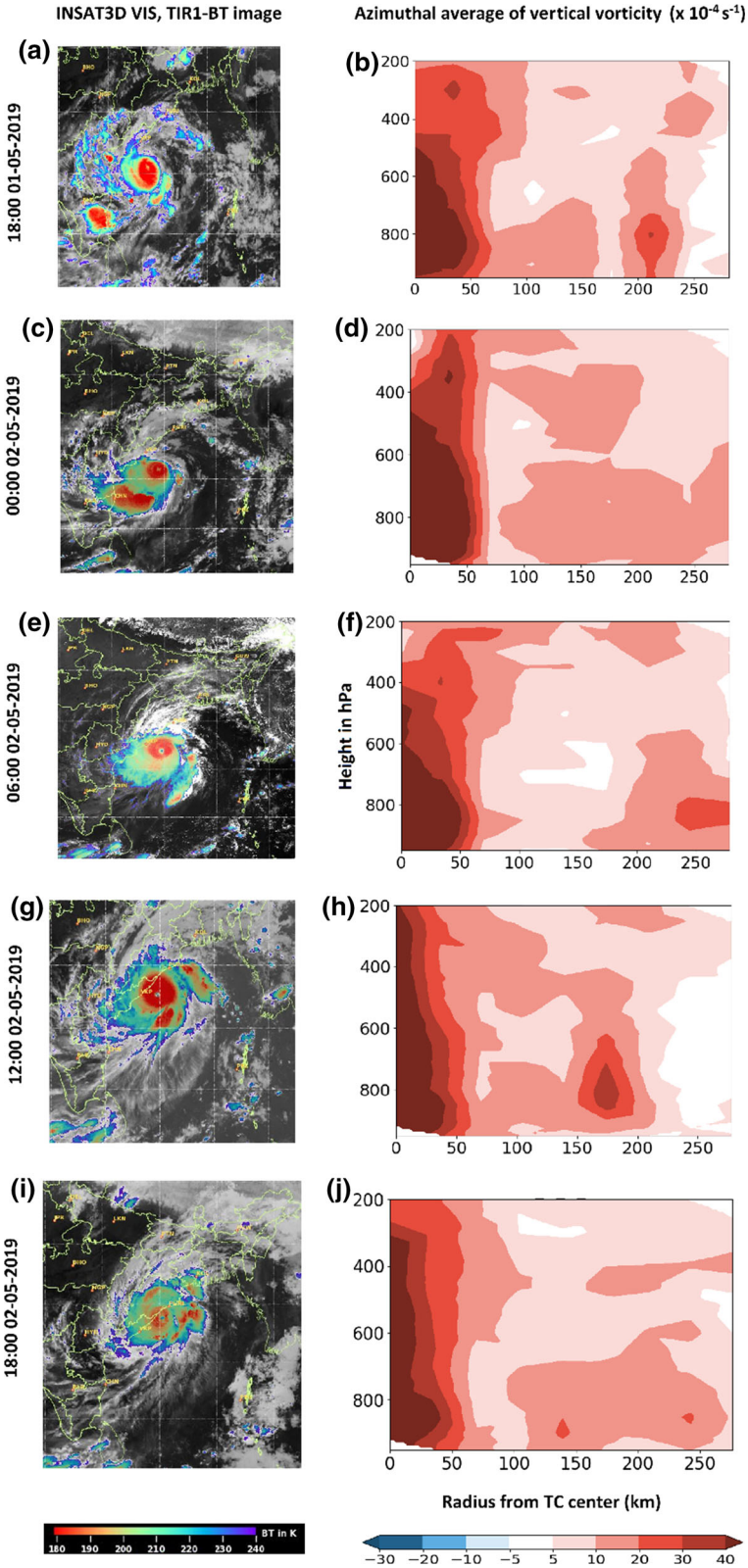

Figure 15. Eyewall replacement cycle depicted by INSAT3D-VIS/IR imagery and azimuthal average of vertical vorticity.

system as the TC intensifies. The core portion is separated from the highly sheared region by a thin annular neutral section characterised by a very low (–5 to 5 × 10^{-7} s^{-2}) OW parameter value where the vorticity and deformation term balance. From the deep depression (DD) stage, the core portion starts getting vorticity dominated and strengthens with time. At the VSCS stage of TC Fani and

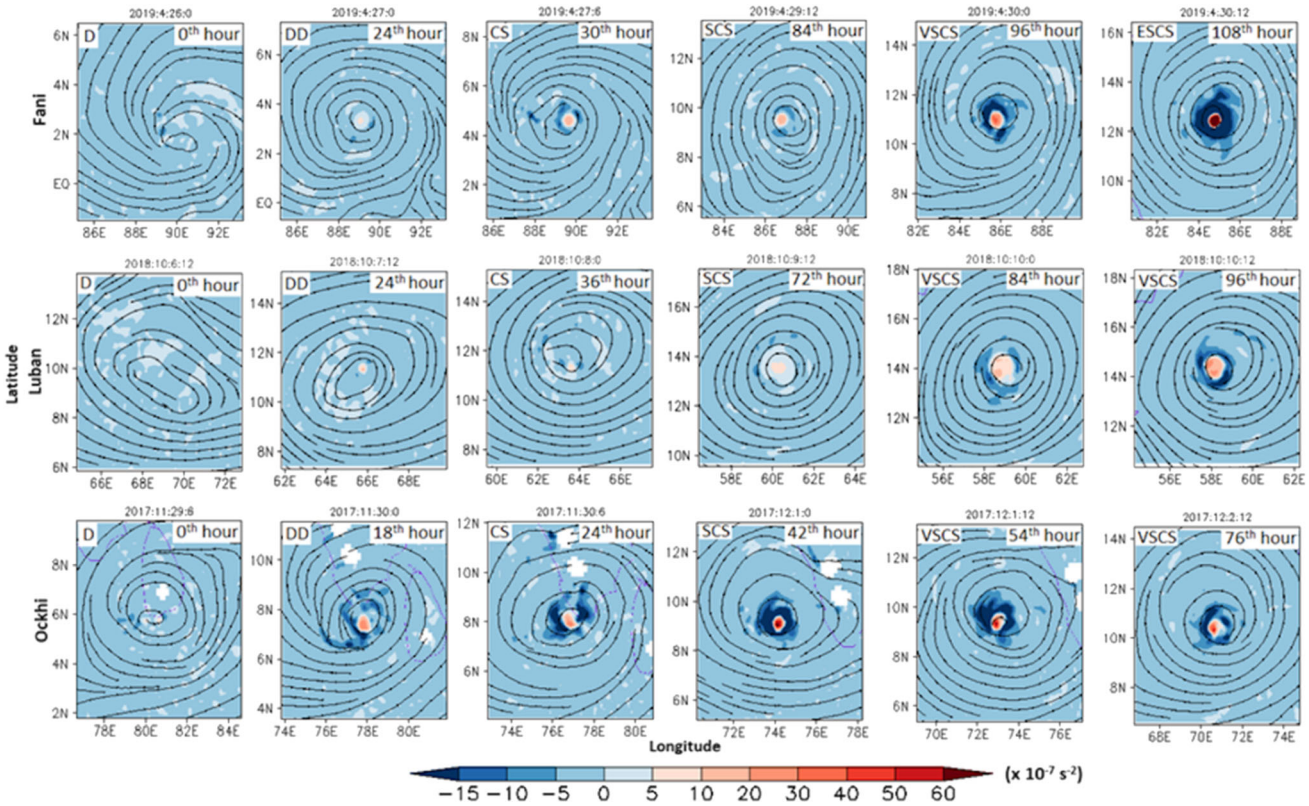

Figure 16. Spatial distribution of OW parameters ($\times 10^{-7}$ s^{-2}) of TC Fani (first row), Luban (second row), and Ockhi (third row).

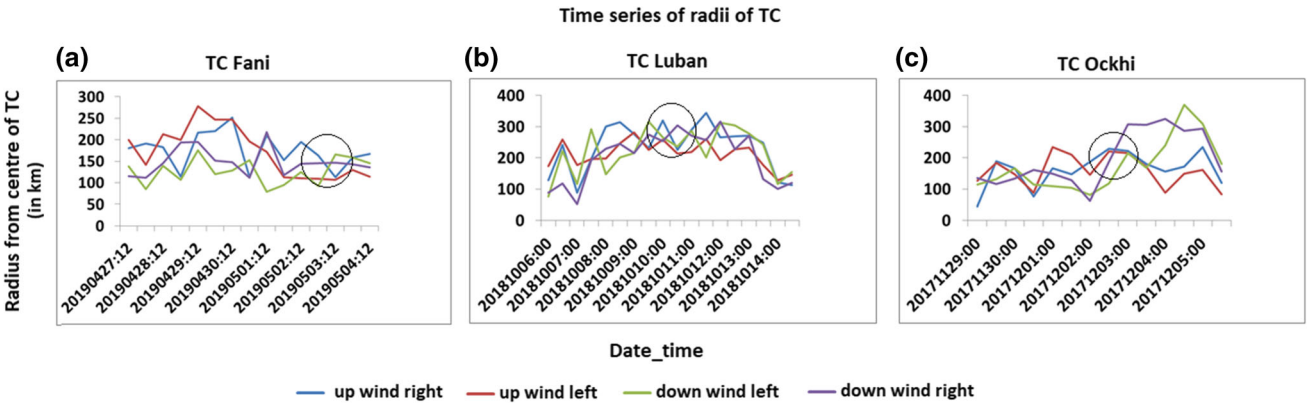

Figure 17. Evolution of radii (km) from the centre of TC Fani **(a)**, Luban **(b)**, Ockhi **(c)** in the four quadrants of the TCs (blue line: upwind right, red line: upwind left, green line: downwind left, and violet line: downwind right). The circle represents the maximum intensified (ESCS: for Fani, VSCS: for Luban and Ockhi) stage of the TCs.

Ockhi, the OW parameter shows a value up to 50 $\times$ 10^{-7} s^{-2}, and that of TC Luban is 30 $\times$ 10^{-7} s^{-2}. TC Fani is attributed by OW parameter above 60 $\times$ 10^{-7} s^{-2} at the ESCS stage. The increasing OW parameter value in the inner core region indicates an enhancement in the rotating updraft, strengthening the TC column.

Stern *et al.* (2015) and Smith and Montgomery (2015) have challenged the convective ring axisymmetric model due to the contribution of the asymmetric framework in TC development. As seen in figure 16, the convection and deformation-dominated regions were organised in an asymmetric pattern. Therefore, the distance of a point with $\zeta = 1 \times 10^{-5}$ s^{-1} from the TC centre (radii of the cyclone) differs in all four quadrants. They are shown in figure 17, which shows that the simulated radii have shown reasonably different values at different quadrants, indicating the asymmetric structure of simulated TCs. The asymmetric and

axisymmetric structures at various stages of TCs have been simulated well in the high-resolution mesoscale analysis. In the case of Fani, the radius in upwind right and left quadrants increased sharply after the CS stage (29 April 2019) with a simultaneous decrease in the left and right downwind quadrants (figure 17a). Similarly, for TC Ockhi (figure 17c), after the CS stage (1 Dec 2017), the radius in upwind quadrants increases while the radius in the downwind quadrant decreases. When TC intensified to the MI stages (TC Fani: 2 May 2019, TC Luban: 10 Oct 2018, TC Ockhi: 02 Dec 2017), they tended to attain symmetric structures as indicated by reducing differences of magnitudes of radius from different quadrants. As discussed in the previous section, during the RI stage of all three cyclones showed asymmetric convection around the centre and quasi-symmetric wind streamlines around the centre. Such an asymmetricity of inner core convection is associated with increasing the available potential energy, which in turn increases the kinetic energy, leading to RI (Callaghan 2017; Geetha and Balachandran 2020). Yu *et al.* (2021) suggested that increased tangential wind and BL updrafts in the 'left-to-shear' sector lead to an asymmetric response in a sheared TC. As per the current study, the structure of the TCs attained symmetry when they underwent the MI phase of their life. Our present study suggests that the structures of the systems are asymmetric during their development, which helped the system to gain the RI phase by transforming available energies, and gradually, the TCs attained symmetry in convective patterns during the MI phase of the system. The initial development of TC Ockhi was cognate by axisymmetrization of the TC vortex, which could be caused by near eyewall vortex Rossby waves (Geetha and Balachandran 2020). The RI phase was associated with non-uniform heating in the vertical direction associated with latent heat release due to convection.

4. Conclusions

For improving the forecast skill of TC intensity, it is prime to understand the internal dynamics of factors controlling TC evolution. Also, the studies have raised concerns about the theoretical framework of intensification of TCs. The representing intensity of TC in terms of maximum wind radius has limitations as it is not materially conserved quantity and is not fundamental to the spin-up process. Nevertheless, the physical mechanism involved in the TC intensification process needs a better theoretical understanding and requires more investigation. Therefore, in this work, we have developed high-resolution analysis to examine the dynamics and thermodynamics of vortex evolution, quadrant-wise radii evolution, warm-core formation and strengthening (intensification), and deformation *vs.* rotation during the life cycle of TCs Fani, Luban, and Ockhi.

In this study, it has been observed that a CAPE value of 1000 Jkg^{-1} ensured the thermodynamic favourability to develop a buoyant updraft for 48 hrs before cyclogenesis and during their lifespan. The CAPE distribution at the BL of TC was highly correlated with the evolution of azimuthal-mean of maximum tangential wind (spin-up) at 850 hPa. The ζ is developed from the lower troposphere to the upper troposphere with the intensification of the TC. A well-formed vortex column throughout the tropospheric height with ζ value above 40×10^{-4} s^{-1} is observed at the MI stage. The unorganised, weak, discontinuous vertical columns of vortex became organised around the eye with intense vertical velocity throughout the column after RI. The radius-wise axisymmetric formation of TCs was observed when they attained maximum intensity, whereas at lower intensities, the asymmetric interaction played a dominant role. The vorticity budget analysis indicated that the relative vorticity tendency was higher throughout the tropospheric layers when Fani underwent RI. For TC Luban and Ockhi, the relative vorticity maxima were observed between the surface to the nearly middle-tropospheric region before attaining the RI. The strengthening of the relative vorticity tendency terms was triggered by vertical stretching of vortex up to upper troposphere in case of TC Fani and lower and middle tropospheric advection in case of TCs Luban and Ockhi. The sufficient magnitude of vorticity tendencies, low frictional and subgrid processes in the lower levels, and the high advection of vorticity above the middle troposphere contributed further in attaining the RI.

The release of CAPE in the presence of nearly saturated middle-level RH causes intense diabatic heating that increases low-level convergence and upper-level divergence for TC Fani and Luban, and these systems have undergone RI. The upper-level diagnostics by Sear and Velden (2014) point to regions of low inertial stability, providing favourable 'soft spots' for potential mass evacuation from

intense core convection. Once it is linked to environmental flow, it provides an effective mass transit from the developing disturbance and helps to maintain the circulations. In the case of TC Ockhi, there was a decrease in upper troposphere divergence during the first RI. This reduction in ventilation flow in the upper level helped accumulate moisture in TC's core region. Later on, the moisture-enriched lower-middle troposphere helped in very strong diabatic heating through the release of CAPE and caused second RI and then MI.

Moreover, the small variation in θ_{ed} throughout these systems' life cycles created favourable conditions for the sustenance of deep convection in the core region and heat supply to the system. The large radial and vertical gradients of the diabatic heating rate favoured the transverse circulation (Wang 2012). In the present case study, the strong vertical gradient of the diabatic heating in the lower troposphere concentrates acts positively to concentrate the radial inflow near the surface, intensifying the tangential circulation. The RI caused cyclonic circulations of three cyclones to extend up to the upper troposphere. Spatial distributions of OW parameter show that TC core portion began vorticity dominated suppressing the strain dominated surrounding from the DD stage. The evolution of dynamical and thermodynamical parameters indicated vortex stretching in the bottom-up mechanism, and the developed positive feedback of diabatic heating, baroclinic instability, increased vertical velocity, and continuous vertical moisture transport and strengthening warm-core are responsible for the intensification of TCs.

Acknowledgements

The authors are thankful to Dr Amit Kumar Patra and Prof V K Dadhwal, Directors, NARL, and IIST, for their support and guidance. The authors are also grateful to the Space Applications Centre, Ahmedabad, for providing SCATSAT1 scatterometer data. They also would like to thank KNMI for distributing ASCAT data and the Global Tropical Moored Buoy Array Project Office by NOAA Pacific Marine Environmental Laboratory (PMEL) for RAMA buoy data. The authors also acknowledge Remote Sensing Systems for Windsat data and are grateful to NCAR for providing the WRF model and WRFDA modelling system. Finally, the authors are thankful to NCEP and NCAR for providing GFS and GDAS radiance datasets for generating high-resolution mesoscale analysis.

Author statement

AM: Simulations, data analysis, visualisation, writing initial manuscript draft; AK: conception, manuscript draft revision, supervision; JB: data assimilation experiments, manuscript draft revision, supervision; KS: methodology, analysis manuscript draft revision, supervision; AP: visualisation; GK: manuscript draft revision, supervision; and RG: manuscript draft revision, supervision.

References

Barker D M, Huang W, Guo Y R, Bourgeois A J and Xiao Q N 2004 A three-dimensional variational data assimilation system for MM5: Implementation and initial results; *Mon. Weather Rev.* **132** 897–914.

Bell M M and Montgomery M T 2010 Sheared deep vortical convection in pre-depression Hagupit during TCS08: Deep convection in hagupit during TCS08; *Geophys. Res. Lett.* **37(6)**, https://doi.org/10.1029/2009GL042313.

Bhalachandran S, Nadimpalli R, Osuri K K, Marks F D, Gopalakrishnan S, Subramanian S, Mohanty U C and Niyogi D 2019 On the processes influencing rapid intensity changes of tropical cyclones over the Bay of Bengal; *Sci. Rep.* **9(1)** 1–14, https://doi.org/10.1038/s41598-019-40332-z.

Bhate J, Munsi A, Kesarkar A K, Kutty G and Deb S K 2021 Impact of assimilation of satellite retrieved ocean surface winds on the tropical cyclone simulations over the north Indian Ocean; *Earth Space Sci.* **8(8)**, https://doi.org/10.1029/2020EA001517.

Bister M and Emanuel K A 1998 Dissipative heating and hurricane intensity; *Meteorol. Atmos. Phys.* **65** 233–240, https://doi.org/10.1007/BF01030791.

Callaghan J 2017 Asymmetric inner core convection leading to tropical cyclone intensification; *Trop. Cyclone Res. Rev.* **6** 55–66, https://doi.org/10.6057/2017TCRRh3.02.

Carr L III and Elsberry R L 1990 Observational evidence for predictions of tropical cyclone propagation relative to environmental steering; *J. Atmos. Sci.* **47** 542–546.

Chan J C 1985 Tropical cyclone activity in the northwest Pacific in relation to the El Niño/Southern Oscillation phenomenon; *Mon. Weather Rev.* **113** 599–606.

Chen X, Zhang J A and Marks F D 2019 A thermodynamic pathway leading to rapid intensification of tropical cyclones in shear; *Geophys. Res. Lett.* **46** 9241–9251.

DeMaria M, Sampson C R, Knaff J A and Musgrave K D 2014 Is tropical cyclone intensity guidance improving?; *Bull. Am. Meteorol.* **95** 387–398, https://doi.org/10.1175/BAMS-D-12-00240.1.

Ditchek S D, Nelson T C, Rosenmayer M and Corbosiero K L 2017 The relationship between tropical cyclones at genesis

and their maximum attained intensity; *J. Clim.* **30** 4897–4913, https://doi.org/10.1175/JCLI-D-16-0554.1.

Dunkerton T J, Montgomery M and Wang Z 2009 Tropical cyclogenesis in a tropical wave critical layer: Easterly waves; *Atmos. Chem. Phys.* **9** 5587–5646.

Elhmaïdi D, Provenzale A and Babiano A 1993 Elementary topology of two-dimensional turbulence from a Lagrangian viewpoint and single-particle dispersion; *J. Fluid Mech.* **257** 533–558, https://doi.org/10.1017/S0022112093003192.

Emanuel K, Desautels C, Holloway C and Korty R 2004 Environmental control of tropical cyclone intensity; *J. Atmos. Sci.* **61(7)** 843–858.

Geetha B and Balachandran S 2016 Diabatic heating and convective asymmetries during rapid intensity changes of tropical cyclones over North Indian Ocean; *Trop. Cyclone Res. Rev.* **5(1–2)** 32–46.

Geetha B and Balachandran S 2020 Development and rapid intensification of tropical cyclone OCKHI (2017) over the North Indian Ocean; *J. Atmos. Res.* **3(3)**.

Gjorgjievska S and Raymond D J 2014 Interaction between dynamics and thermodynamics during tropical cyclogenesis; *Atmos. Chem. Phys.* **14** 3065–3082, https://doi.org/10.5194/acp-14-3065-2014.

Gray W M 1968 Global view of the origin of tropical disturbances and storms; *Mon. Weather Rev.* **96** 669–700.

Gray W M 1975 Tropical cyclone genesis. Department of Atmospheric Science, Paper No. 234, Colorado State University, Fort Collins, CO, 121p, https://mountainscholar.org/bitstream/handle/10217/247/0234_Bluebook.pdf;sequence=1.

Hack J J and Schubert W H 1986 Nonlinear response of atmospheric vortices to heating by organised cumulus convection; *J. Atmos. Sci.* **43** 1559–1573.

Hanley D, Molinari J and Keyser D 2001 A composite study of the interactions between tropical cyclones and upper-tropospheric troughs; *Mon. Weather Rev.* **129(10)** 2570–2584.

Hendricks E A, Montgomery M T and Davis C A 2004 The role of 'Vortical' hot towers in the formation of tropical cyclone Diana (1984); *J. Atmos. Sci.* **61(11)** 1209–1232.

Hendricks E A, Peng M S, Fu B and Li T 2010 Quantifying environmental control on tropical cyclone intensity change; *Mon. Weather Rev.* **138** 3243–3271, https://doi.org/10.1175/2010MWR3185.1.

Ito K, Wu C C, Chan K T, Toumi R and Davis C 2020 Recent progress in the fundamental understanding of tropical cyclone motion; *J. Meteorol. Soc. Jpn. Ser II.*

Jaiswal N, Kumar P and Kishtawal C 2019 SCATSAT-1 wind products for tropical cyclone monitoring, prediction and surface wind structure analysis; *Curr. Sci.* **117** 983–992.

Jaiswal N, Deb S K and Kishtawal C M 2022 Intensification of tropical cyclone FANI observed by INSAT-3DR rapid scat data; *Theor. Appl. Climatol.*, https://doi.org/10.21203/rs.3.rs-368454/v1.

Jung J H and Arakawa 2007 A three-dimensional anelastic model based on the vorticity equation; *Mon. Weather Rev.* **136** 276–294, https://doi.org/10.1175/2007MWR295.1.

Kaplan J, DeMaria M and Knaff J A 2010 A revised tropical cyclone rapid intensification index for the Atlantic and eastern North Pacific basins; *Weather Forecast.* **25** 220–241.

Kieu C Q and Zhang D L 2009 An analytical model for the rapid intensification of tropical cyclones; *Quart. J. Roy. Meteorol. Soc.* **135** 1336–1349.

Kotal S and Bhowmik S R 2013 Large-scale characteristics of rapidly intensifying tropical cyclones over the Bay of Bengal and a rapid intensification (RI) index; *Mausam* **64** 13–24.

Kutty G and Gohil K 2017 The role of mid-level vortex in the intensification and weakening of tropical cyclones; *J. Earth Syst. Sci.* **126(7)** 1–12, https://doi.org/10.1007/s12040-017-0879-y.

Lee M and Frisius T 2018 On the role of convective available potential energy (CAPE) in tropical cyclone intensification; *Tellus a: Dyn. Meteorol. Oceanogr.* **70(1)** 1–18, https://doi.org/10.1080/16000870.2018.1433433.

Mapes B E and Houze R A Jr 1995 Diabatic divergence profiles in western Pacific mesoscale convective systems; *J. Atmos. Sci.* **52(10)** 1807–1828.

Merrill R T 1988 Environmental influences on hurricane intensification; *J. Atmos. Sci.* **45** 1678–1687.

Miyamoto Y and Nolan D S 2018 Structural changes preceding rapid intensification in tropical cyclones as shown in a large ensemble of idealised simulations; *J. Atmos. Sci.* **75** 555–569.

Miyamoto Y and Takemi T 2015 A triggering mechanism for rapid intensification of tropical cyclones; *J. Atmos. Sci.* **72** 2666–2681.

Mohanty U, Nadimpalli R and Mohanty S 2021 Understanding the rapid intensification of tropical cyclone Titli using Hurricane WRF model simulations; *Mausam* **72** 167–176.

Molinari J and Vollaro D 2010 Rapid intensification of a sheared tropical storm; *Mon. Weather Rev.* **138** 3869–3885.

Montgomery M T and Kallenbach R J 1997 A theory for vortex Rossby-waves and its application to spiral bands and intensity changes in hurricanes; *Quart. J. Roy. Meteorol. Soc.* **123** 435–465.

Montgomery M T, Nicholls M E, Cram T A and Saunders A B 2006 A vortical hot tower route to tropical cyclogenesis; *J. Atmos. Sci.* **63** 355–386, https://doi.org/10.1175/JAS3604.1.

Munsi A, Kesarkar A, Bhate J, Panchal A, Singh K, Kutty G and Giri R 2021 Rapidly intensified, long duration North Indian Ocean tropical cyclones: Mesoscale downscaling and validation; *Atmos. Res.* **259** 105678.

Nadimpalli R, Mohanty S, Pathak N, Osuri K K, Mohanty U C and Chatterjee S 2021 Understanding the characteristics of rapid intensity changes of tropical cyclones over North Indian Ocean; *SN Appl. Sci.* **3** 1–12.

Peng M S, Jeng B F and Williams R T 1999 A numerical study on tropical cyclone Intensification. Part I: Beta effect and mean flow effect; *J. Atmos. Sci.* **56(10)** 1404–1423.

Persing J, Montgomery M T, McWilliams J C and Smith R K 2013 Asymmetric and axisymmetric dynamics of tropical cyclones; *Atmos. Chem. Phys.* **13** 12,299–12,341, https://doi.org/10.5194/acp-13-12299-2013.

Rajasree V P M, Kesarkar A P, Bhate J N, Singh V, Umakanth U and Varma T H 2016a A comparative study on the genesis of North Indian Ocean tropical cyclone Madi (2013) and Atlantic Ocean tropical cyclone Florence (2006); *J. Geophys. Res. Atmos.* **121(23)** 13,826–13,858, https://doi.org/10.1002/2016JD025412.

Rajasree V P M, Kesarkar A P, Bhate J N, Umakanth U, Singh V and Varma T H 2016b Appraisal of recent theories to understand cyclogenesis pathways of tropical cyclone Madi (2013); *J. Geophys. Res. Atmos.* **121(15)** 8949–8982, https://doi.org/10.1002/2016JD025188.

Rajasree V P M, Routray A, George J P, Kumar S and Kesarkar A P 2021 Study of cyclogenesis of developing and

non-developing tropical systems of NIO using NCUM forecasting system; *Meteorol. Atmos. Phys.* **133** 379–397, https://doi.org/10.1007/s00703-020-00756-z.

Routray A, Lodh A, Dutta D and George J P 2020 Study of an extremely severe cyclonic storm 'Fani' over Bay of Bengal using regional NCUM modeling system: A case study; *J. Hydrol.* **590** 125357, https://doi.org/10.1016/j.jhydrol.2020.125357.

Sanger N T, Montgomery M T, Smith R K and Bell M M 2014 An observational study of tropical cyclone spin-up in super typhoon Jangmi (2008) from 24 to 27 September; *Mon. Weather Rev.* **142** 3–28, https://doi.org/10.1175/MWR-D-12-00306.1.

Sear J and Velden C S 2014 Investigating the role of upper levels in tropical cyclone genesis; *Trop. Cyclone Res. Rev.* **3** 91–110.

Shapiro L J and Willoughby H E 1982 The response of balanced hurricanes to local sources of heat and momentum; *J. Atmos. Sci.* **39** 378–394.

Sheng C, Wu G, Tang Y, He B, Xie Y, Ma T, Ma T, Li J, Bao Q and Liu Y 2021 Characteristics of the potential vorticity and its budget in the surface layer over the Tibetan plateau; *Int. J. Climatol.* **41** 439–455, https://doi.org/10.1002/joc.6629.

Singh V K and Roxy M 2022 A review of the ocean-atmosphere interactions during tropical cyclones in the north Indian Ocean; *Earth Sci. Rev.* 103967.

Singh K, Panda J, Sahoo M and Mohapatra M 2019 Variability in tropical cyclone climatology over North Indian Ocean during the period 1891 to 2015; *Asia-Pac. J. Atmos. Sci.* **55** 269–287.

Singh V K, Roxy M and Deshpande M 2020 The unusual long track and rapid intensification of very severe cyclone Ockhi; *Curr. Sci.* **119** 771–779.

Singh V, Konduru R T, Srivastava A K, Momin I M, Kumar S, Singh A K, Bisht D S, Tiwari S and Sinha A K 2021 Predicting the rapid intensification and dynamics of pre-monsoon extremely severe cyclonic storm 'Fani' (2019) over the Bay of Bengal in a 12-km global model; *Atmos. Res.* **247(6)** 105222, https://doi.org/10.1016/j.atmosres.2020.105222.

Smith R K and Montgomery M T 2015 Toward clarity on understanding tropical cyclone intensification; *J. Atmos. Sci.* **72** 3020–3031, https://doi.org/10.1175/JAS-D-15-0017.1.

Smith R K and Montgomery M T 2016 The efficiency of diabatic heating and tropical cyclone intensification; *Quart. J. Roy. Meteorol. Soc.* **142** 2081–2086.

Stern D P, Vigh J L, Nolan D S and Zhang F 2015 Revisiting the relationship between eyewall contraction and intensification; *J. Atmos. Sci.* **72** 1283–1306, https://doi.org/10.1175/JAS-D-14-0261.1.

Sun Y, Zhong Z, Li T, Yi L, Hu Y, Wan H, Chen H, Liao Q, Ma C and Li Q 2017 Impact of ocean warming on tropical cyclone size and its destructiveness; *Sci. Rep.* **7(1)** 1–10.

Tory K J and Frank W M 2010 Tropical cyclone formation. In: *Global perspectives on tropical cyclones: From science to mitigation* (ed.) Chan C L and Kepert J D, pp. 55–91.

Vigh J L and Schubert W H 2009 Rapid development of the tropical cyclone warm core; *J. Atmos. Sci.* **66** 3335–3350, https://doi.org/10.1175/2009JAS3092.1.

Wang Z 2012 Thermodynamic aspects of tropical cyclone formation; *J. Atmos. Sci.* **69** 2433–2451, https://doi.org/10.1175/JAS-D-11-0298.1.

Wang Z 2014 Role of cumulus congestus in tropical cyclone formation in a high-resolution numerical model simulation; *J. Atmos. Sci.* **71** 1681–1700, https://doi.org/10.1175/JAS-D-13-0257.1.

Wang B and Chan J C L 2002 How strong ENSO events affect tropical storm activity over the western north Pacific; *J. Clim.* **15(13)** 1643–1658.

Wang Y and Wu C C 2004 Current understanding of tropical cyclone structure and intensity changes: A review; *Meteorol. Atmos. Phys.* **87** 257–278, https://doi.org/10.1007/s00703-003-0055-6.

Wang Z, Montgomery M and Dunkerton T 2010 Genesis of pre–hurricane Felix (2007). Part II: warm core formation, precipitation evolution, and predictability; *J. Atmos. Sci.* **67** 1730–1744.

Wang X, Zhou X, Zuyu T and Hua L 2016 Discussion on the complete-form vorticity equation and slantwise vorticity development; *J. Meteorol. Res.* **30(1)** 67–75.

Williams E and Renno N 1993 An analysis of the conditional instability of the tropical atmosphere; *Mon. Weather Rev.* **121** 21–36.

Willoughby H E 1979 Forced secondary circulations in hurricanes; *J. Geophys. Res. Oceans* **84(C6)** 3173–3183, https://doi.org/10.1029/JC084iC06p03173.

Willoughby H, Clos J and Shoreibah M 1982 Concentric eye walls, secondary wind maxima, and the evolution of the hurricane vortex; *J. Atmos. Sci.* **39** 395–411.

Wu R and Juan Fang 2001 Mechanism of balanced flow and frontogenesis; *Adv. Atmos. Sci.* **18** 323–334.

Wu L, Su H, Fovell G, Wang B, Shen J T, Kahn B H, Hristova-Veleva S M, Lambrigtsen B H, Fetzer E J and Jiang J H 2012 Relationship of environmental relative humidity with North Atlantic tropical cyclone intensity and intensification rate; *Geophys. Res. Lett.* **39** L20809, https://doi.org/10.1029/2012GL053546.

Wu Y, Chen S, Li W, Fang R and Liu H 2020 Relative vorticity is the major environmental factor controlling tropical cyclone intensification over the Western North Pacific; *Atmos. Res.* **237** 104874, https://doi.org/10.1016/j.atmosres.2020.104874.

Xie Y, Wu G, Liu Y, Huang J and Nie H 2021 A dynamic and thermodynamic coupling view of the linkages between Eurasian cooling and Arctic warming; *Clim. Dyn.*, https://doi.org/10.1007/s00382-021-06029-8.

Yan Z, Ge X, Peng M and Li T 2019 Does monsoon gyre always favour tropical cyclone rapid intensification?; *Quart. J. Roy. Meteorol. Soc.* **145** 2685–2697.

Yu C L, Didlake A C, Kepert J D and Zhang F 2021 Investigating axisymmetric and asymmetric signals of secondary eyewall formation using observations-based modeling of the tropical cyclone boundary layer; *J. Geophys. Res. Atmos.* **126** e2020JD034027, https://doi.org/10.1029/2020JD034027.

Zhang D L and Chen H 2012 Importance of the upper-level warm core in the rapid intensification of a tropical cyclone; *Geophys. Res. Lett.* **39(2)**, https://doi.org/10.1029/2011GL050578.

Zhang R, Huangfu J and Hu T 2019 Dynamic mechanism for the evolution and rapid intensification of Typhoon Hato (2017); *Atmos. Sci. Lett.* **20(8)** e930.

Corresponding editor: Parthasarathi Mukhopadhyay